Scientific Research Publishing

Atmospheric and Climate Sciences, 2025, 15(4), 908-940
https://www.scirp.org/journal/acs
ISSN Online: 2160-0422
ISSN Print: 2160-0414

High-Resolution Climate Modeling of Deforestation Scenarios along the BR-319 Highway

Jerfferson Lobato dos Santos[1,2,3], Francis Wagner Silva Correia[2,4,5], Weslley de Brito Gomes[5], Leonardo Alves Vergasta[5], Paulo Maurício A. Graça[6], Philip M. Fearnside[1,6]

[1]Postgraduate Program in Climate and the Environment, National Institute of Amazonian Research (INPA), Manaus, Amazonas, Brazil
[2]Postgraduate Program in Climate and the Environment, State University of Amazonas (UEA), Manaus, Amazonas, Brazil
[3]Brazilian Institute of the Environment and Renewable Natural Resources (IBAMA), SCEN trecho 2, Brasília, Federal District, Brazil
[4]School of Technology, State University of Amazonas (UEA), Manaus, Amazonas, Brazil
[5]Laboratory of Terrestrial Climate System Modeling (LABCLIM), State University of Amazonas (UEA), Manaus, Amazonas, Brazil
[6]Department of Environmental Dynamics, National Institute of Amazonian Research (INPA), Manaus, Amazonas, Brazil
Email: Jerfferson.santos@ibama.gov.br

How to cite this paper: dos Santos, J.L., Correia, F.W.S., Gomes, W.B., Vergasta, L.A., Graça, P.M.A. and Fearnside, P.M. (2025) High-Resolution Climate Modeling of Deforestation Scenarios along the BR-319 Highway. *Atmospheric and Climate Sciences*, **15**, 908-940.
https://doi.org/10.4236/acs.2025.154046

Received: August 22, 2025
Accepted: October 11, 2025
Published: October 14, 2025

Abstract

This study investigates the impacts of deforestation within the influence area of the BR-319 highway on local climate conditions following its planned reconstruction. High-resolution climate modeling indicates that mean air temperature may increase by up to 0.7˚C under the paved-road scenario (BAU_2) by 2100, with local increases exceeding 2.5˚C in deforested regions during the dry season. Precipitation is projected to rise by an average of up to 0.5 mm·day^{-1}, with local increases above 2.5 mm·day^{-1} in fragmented landscapes. However, this effect is likely temporary and may shift to declining rainfall as deforestation consolidates into large continuous areas. These effects are driven by reduced evapotranspiration, increased surface temperatures, and changes in atmospheric circulation patterns. Such alterations result in greater moisture convergence over deforested zones, thereby influencing the regional hydrological cycle. The comparison of different deforestation scenarios underscores the significant influence of highway development on local climate. The results highlight the importance of incorporating climate projections into environmental assessments to inform public policy decisions regarding infrastructure projects in the Amazon.

Keywords

Deforestation, Highways, BR-319, Climate Modeling, Land-Use Change

1. Introduction

The Amazon rainforest is widely recognized as a critical environmental asset at local, regional, and global scales [1]. It plays a fundamental role in maintaining the climate system through processes such as carbon storage and absorption, trace gas and aerosol transport, and the recycling of water and nutrients [2]-[4]. Additionally, it contributes to sustaining atmospheric circulation, hydrological regimes, and the conservation of water resources, essential for climate regulation and biodiversity maintenance [5]-[8].

Conversely, deforestation and forest fires have emerged as critical challenges in the Amazon over recent decades, encroaching on large areas of preserved forest and causing substantial environmental and social impacts [9] [10]. These land-use and land-cover changes disrupt the exchange processes of energy, mass, and momentum between the surface and the atmosphere and contribute to global climate change through increased greenhouse gas emissions [11] [12]. Such changes can significantly affect regional and local scales, disturbing the hydrological cycle and intensifying extreme events such as droughts and floods [13]-[15].

Several studies have assessed the impacts of Amazonian land-cover changes on local climate, as well as their influence on regional and global systems [16]-[19]. Overall, these studies have shown that deforestation in the Amazon leads to significant changes in energy, water, and carbon balances, resulting in increased air temperature, reduced precipitation, lower evapotranspiration rates, and greater surface runoff at the regional scale.

To understand and mitigate these impacts, numerical climate modeling has become an essential tool. It allows the simulation of deforestation effects on climate and provides a detailed analysis of how land-cover changes influence meteorological variables and affect sectors such as agriculture, water resources, food security, and public health. This modeling forms a robust foundation for long-term planning and decision-making [20] [21].

Global and regional climate models have advanced significantly in recent years, particularly in the representation of physical, chemical, and biogeochemical processes, as well as in spatial and temporal resolution [22]-[24]. These advances, supported by technological progress and increased computational power, have made climate models more accurate and detailed, enabling the assessment of various deforestation scenarios.

While global circulation models (GCMs) are valuable for capturing macro-scale trends, they operate at coarse spatial resolutions. In contrast, regional climate models (RCMs) provide more detailed representations of climatic conditions by downscaling GCM projections, particularly those related to anthropogenic effects

[21] [25] [26].

In recent decades, studies using climate models to examine deforestation impacts on the Amazonian climate have identified significant disruptions to energy, water, and carbon cycles, along with changes in atmospheric circulation, affecting ecosystems and the forest's carbon storage capacity [16]-[19]. These models suggest that deforestation increases temperature and alters precipitation patterns, with the magnitude of impact varying according to deforestation extent [27]-[35]. In smaller deforested areas, precipitation may increase due to changes in air circulation; however, as deforestation expands, rainfall tends to decline, particularly in the "arc of deforestation" in the southern and eastern Amazon [7].

It is important to note that in the early phases of deforestation, especially when shaped by road-driven 'fishbone' patterns, forest fragmentation may lead to localized increases in precipitation. This is due to enhanced mesoscale circulations generated by surface heterogeneity. However, this effect is temporary, as further consolidation of deforestation into large continuous clearings typically results in reduced rainfall. Our study explores this transitional phase in detail.

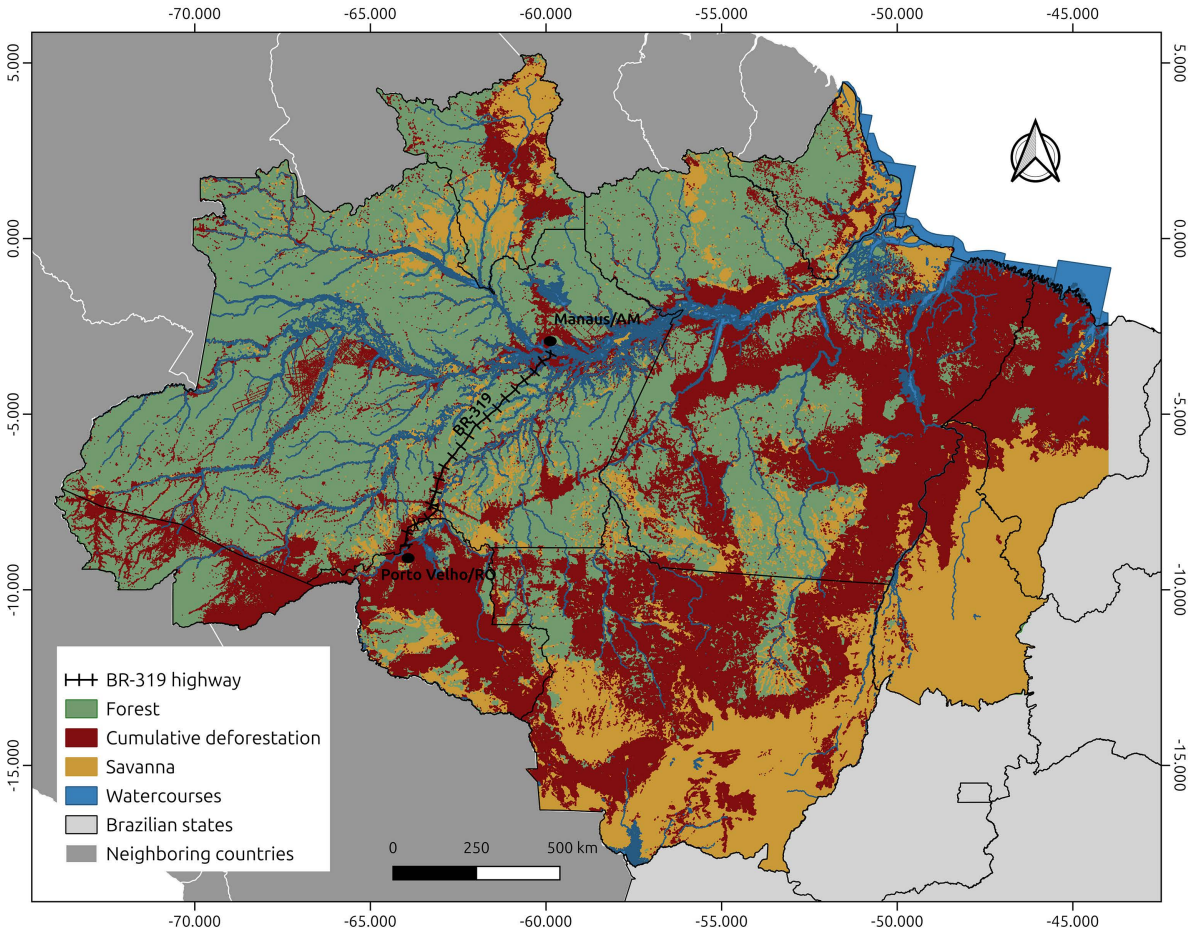

Figure 1. Map of the Brazilian Legal Amazon region showing the BR-319 highway (connecting the cities of Manaus in Amazonas and Porto Velho in Rondônia), along with other major highways and the spatial distribution of cumulative deforestation from 1988 to 2022. Map produced by the authors. Data source: [45].

In Brazil, the planned reconstruction and paving of the BR-319 highway, a long-distance road linking Manaus and Porto Velho across 885 km in the western Amazon (**Figure 1**), has become a subject of debate. Even prior to the road's reconstruction, mere announcements of paving and improvements have triggered irregular land occupation and increased deforestation along the route. These activities include agriculture expansion, extensive cattle ranching, logging, land speculation, and illegal land grabbing in the southern part of Amazonas state [36]-[39].

Effective governance is required to counter these pressures. However, historical evidence suggests that environmental programs often fail to prevent the massive impacts associated with Amazonian highways [40] [41]. A notable example is the failed attempt to control deforestation and illegal occupation along the BR-163 (Santarém-Cuiabá) highway, which sought to halt forest destruction [42]-[44].

The reconstruction of the BR-319 highway may significantly alter the current deforestation pattern by shifting the arc of deforestation[1] northward into the Western Amazon, reaching northern Amazonas state, Roraima, and extending to the Venezuelan border [36] [37] [46]. Furthermore, it would open access to forests in the western part of Amazonas state through the construction of state roads connected to BR-319 [47] [48].

Illegal land occupation and environmental degradation resulting from road reconstruction and paving may drive deforestation further into the Amazon Basin and, consequently, trigger disruptions in the regional climate [47] [49]-[51]. Therefore, understanding the impact of physical environmental changes on the climate, and how these changes in climatic processes may influence biodiversity and local livelihoods, should be a priority for informing measures aimed at mitigating the environmental consequences of human activity.

Considering the ongoing plans to reconstruct and pave the BR-319 highway and the potential impacts of changes in land use and land cover, a key question has emerged within the scientific community: To what extent might the deforestation induced by the reconstruction of BR-319 alter the climate within its area of influence? To address this question, the present study aims to evaluate the potential climatic impacts of deforestation driven by the reconstruction of the BR-319 highway.

2. Materials and Methods

This section presents the methodological approach adopted to evaluate the climatic impact of the reconstruction of the BR-319 highway in its area of influence. The Eta regional climate model was used to perform five numerical experiments simulating different deforestation and road paving scenarios for the years 2050

[1]The "arc of deforestation" is a vast area in the Amazon that has been altered for the establishment of agriculture and cattle ranching. Originating in the eastern and southern portions of the Brazilian Amazon, it is expanding into the southwestern Amazon. In addition to extensive deforestation, this region also has the highest number of land conflicts [52].

and 2100. The model was configured with a horizontal resolution of 3 km and driven by ERA5 reanalysis data along with updated climatological information. Model validation was carried out by comparing the simulations with precipitation and temperature estimates from the Climate Hazards Group InfraRed Precipitation with Station data (CHIRPS) and the South American Mapping of Temperature (SAMeT), respectively.

2.1. Study Area

The study area is based on the investigation proposed by [48], which encompassed the entire state of Amazonas. However, considering the need to use the highest possible spatial resolution and the limitations of computational capacity and processing time, the focus was narrowed to the BR-319 highway and its associated access roads (existing and planned). This configuration was selected to better represent the climatic impact within the largest feasible area for high-resolution simulation. Therefore, the study domain was defined between the geographic coordinates 67˚W to 59˚W and 8˚S to 2˚S (**Figure 2**).

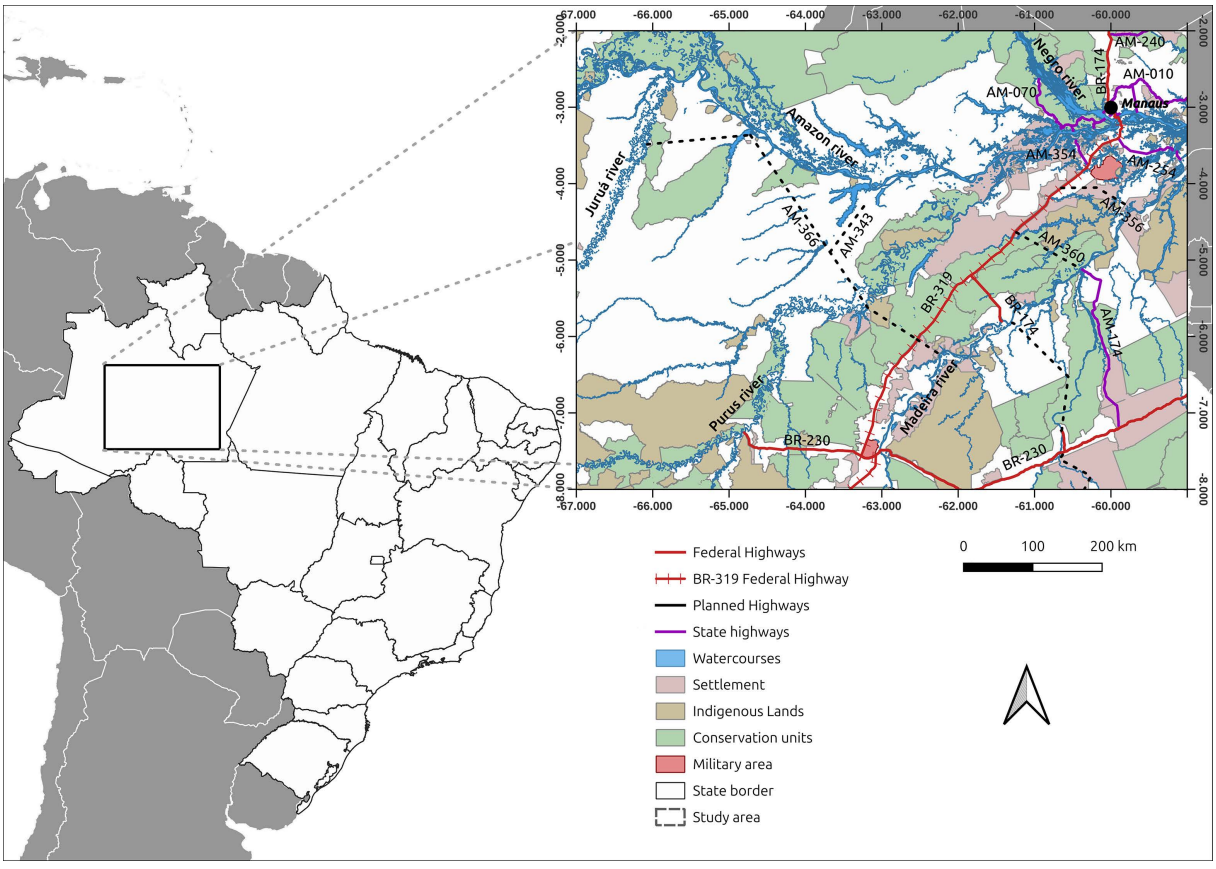

Figure 2. Study area coverage, BR-319 highway, and adjacent existing and planned road network around BR-319, including Federal and State Conservation Units, Indigenous Lands, Federal Settlement Projects, and Military Areas. Map created by the authors. Data sources: [54]-[57].

The study focuses on the impact of the reconstruction of the BR-319 highway,

which is located between the Madeira and Purus river basins, connecting the cities of Manaus and Porto Velho. BR-319 is the main terrestrial access route to the municipal seats of Careiro, Manaquiri, Careiro da Várzea, and Autazes, and it also facilitates access to Humaitá, Lábrea, and Manicoré. It serves as the only land connection to the communities of Vila Realidade (a district of the municipality of Humaitá) and Igapó-Açu (a district of Borba). BR-319 also provides road access to Roraima state via the BR-174 highway, and to Pará state via BR-230 (Transamazon Highway).

The currently existing network of official roads in Amazonas state connected to the 885 km of BR-319 totals 1934 km, comprising the federal highways BR-230 (827 km from Lábrea-AM to the border with Pará), BR-174 (85 km section between BR-319 and Manicoré), and the state highways AM-254 (94 km from BR-319 to Autazes) and AM-354 (43 km from BR-319 to Manaquiri). Additionally, the Amazonas state government has proposed new roads connecting BR-319 to the municipalities of Tapauá, Tefé, Juruá (via AM-366), and Coari (via AM-343), advancing into the area west of the Purus River. This would facilitate deforestation in one of the most pristine forest areas in the state, known as the "Trans-Purus" region [53], which was also included in our modeling framework.

The dominant vegetation types in Amazonas state include dense ombrophilous forest, campinarana (in the far north), open ombrophilous forest, and savanna in the south [54]. In the northern part of the Purus-Madeira interfluve, lowland dense ombrophilous forest predominates, while in the southern part, lowland open ombrophilous forest is more common [54]. The study area features an equatorial rainforest climate (Af) and monsoon climate (Am), according to the Köppen-Geiger classification [58]. The central and western portions experience extremely humid conditions with no dry season, whereas the southern portion has a humid climate with 1 to 3 dry months in the east and south [54]. Due to the high solar radiation received throughout the year, air temperature shows little seasonal variation, except in the far south where frontal systems occur. The mean annual air temperature is approximately 27˚C, and annual rainfall is around 2000 mm [2] [59].

2.2. Deforestation Dynamics Model

The simulated deforestation maps used in this study were generated by Santos *et al.* (2023) and cropped to match the spatial extent proposed here (**Figure 3**). These maps were produced using the DINAMICA-EGO platform (Environment for Geoprocessing Objects) [60].

The modeling approach considered the historical trends of land occupation expansion by different local groups, reflecting the dynamics of land use and conflicts that influence landscape changes along road networks (Business as Usual, BAU) [40] [42] [44]. Therefore, the projections did not assume improved environmental governance or land management practices.

Two environmental forecast scenarios were developed starting from the year

2021, with projections for the years 2050 and 2100: Scenario 1 (BAU_1): BR-319 without asphalt paving (current condition, assuming the reconstruction and paving process remains unapproved); Scenario 2 (BAU_2): BR-319 with paving (assuming paving is authorized and begins in 2025). For additional methodological details, see [48].

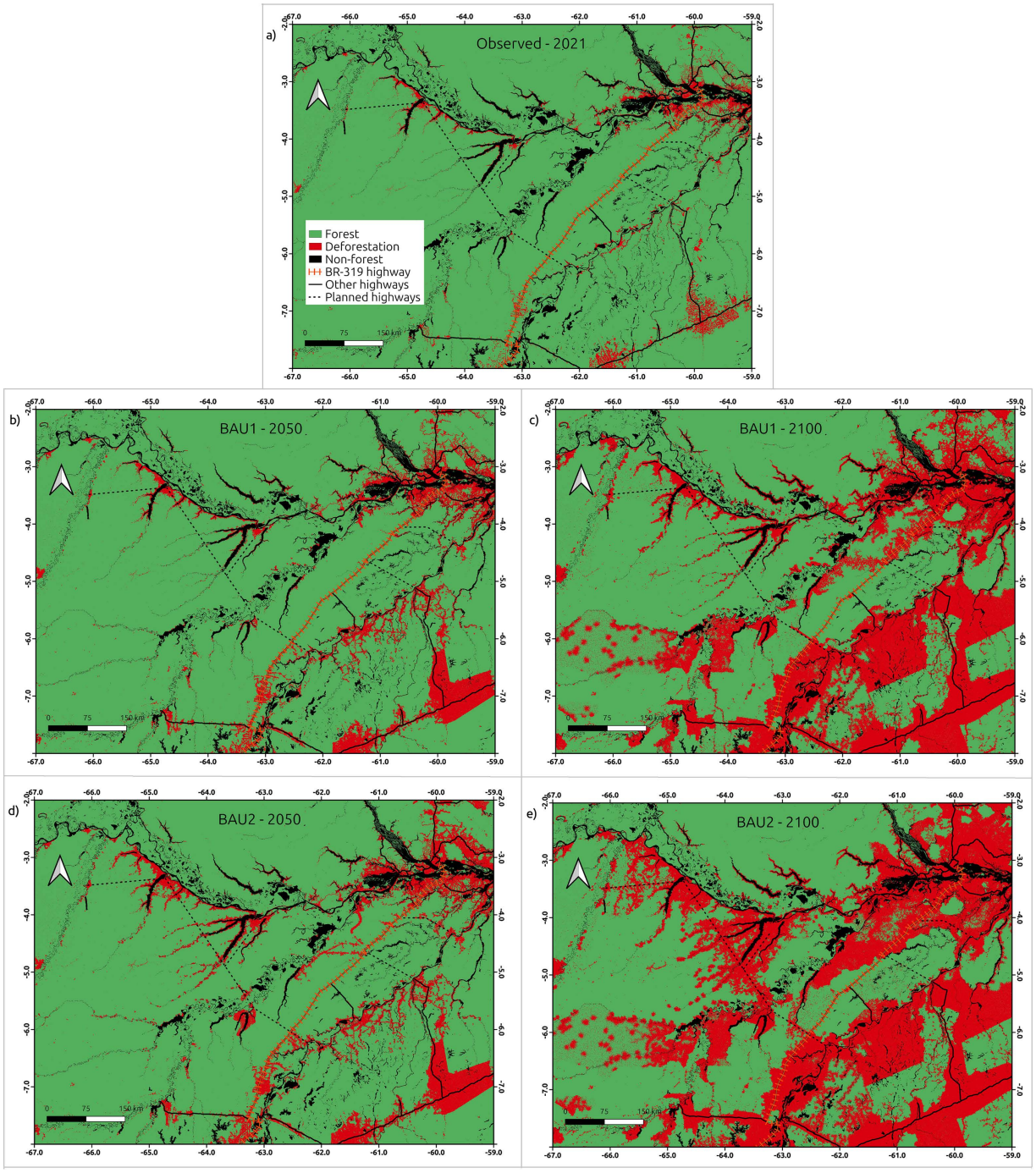

Figure 3. Land-use and land-cover maps used in the climate simulations for the BR-319 highway area of influence: A) control year 2021; B) Scenario 1 (BAU_1-2050), without paving; C) Scenario 1 (BAU_1-2100), without paving; D) Scenario 2 (BAU_2-2050), with paving; and E) Scenario 2 (BAU_2-2100), with paving [48].

2.3. Regional Climate Model Eta

For the climate simulations, the Eta Regional Climate Model from the National Institute for Space Research (INPE) was employed [26] [61]. The Eta model is a limited-area atmospheric model originally developed at the University of Belgrade in collaboration with the Hydrometeorological Institute of Yugoslavia in 1993 [62].

An enhanced version of the model, known as Eta-CPTEC, was developed by the Center for Weather Forecast and Climate Studies (CPTEC) at INPE. This version incorporated significant modifications to improve the representation of climate change interactions in South America [26] [61] [63] [64]. The principles, parameterizations, and configuration settings of the model are described in **Appendix A**.

2.4. Climate Integration Strategy

In this study, five numerical experiments were performed using the Eta regional climate model, named as follows: CNT-2021, BAU_1-2050, BAU_1-2100, BAU_2-2050, and BAU_2-2100. The control experiment (CNT) used vegetation cover data for the Legal Amazon region from the National Institute for Space Research (INPE) and deforestation data from the PRODES project for the baseline year 2021 (INPE, 2021). The other experiments employed deforestation scenarios developed by [48], projected for the years 2050 and 2100, respectively.

Each Eta model experiment consisted of one continuous 10-year integration (120 months), starting at 00:00 UTC on November 1, 2011 (wet season). Each experiment included a spin-up period of one year (12 months).

Initial and boundary atmospheric conditions were derived from ERA5 reanalysis data produced by the European Centre for Medium-Range Weather Forecasts (ECMWF) [65]. These reanalyses have a horizontal resolution of $0.25^\circ \times 0.25^\circ$ and cover the domain from 57˚S to 79.5˚N and from 180˚W to 180˚E, encompassing all continents except Antarctica. The data are available at: https://www.ecmwf.int/en/forecasts/datasets/browse-reanalysis-datasets.

The model assimilated the reanalysis fields every six hours via dynamic downscaling. Sea surface temperature (SST) values were derived from monthly ECMWF reanalysis means and were updated daily using linear interpolation. Initial soil moisture and surface albedo conditions were based on monthly climatology for the first month of integration and on seasonal climatology, respectively.

For this study, the Eta-ERA5 model was configured with a horizontal resolution of 3 km, 38 vertical layers, a timestep of 10 seconds, and a spatial domain from 67.0˚W to 59.0˚W and from 8.0˚S to 2.0˚S. During the numerical integrations, the atmospheric CO_2 concentration in the model was held constant at the mean value of 414 ppmv, since the primary focus was to analyze climate changes resulting specifically from the BR-319 highway project.

Validation of the Eta Regional Model

To assess the performance of the Eta regional model in simulating the climate of

the study area, rainfall estimates from CHIRPS (Climate Hazards Group InfraRed Precipitation with Station data) [66] and temperature data from SAMeT (South American Mapping of Temperature) [67] were used. The validation was based on mean seasonal fields for the wet season (austral summer: December-January-February, DJF) and the dry season (austral winter: June-July-August, JJA). For the quantitative evaluation of the Eta model performance, the following statistical metrics were applied: bias and root mean square error (RMSE).

3. Results and Discussion

The results presented here aim to assess the potential climate impacts of deforestation associated with the reconstruction of the BR-319 highway within the study area. In environmental impact assessments for large-scale infrastructure projects, environmental forecasting plays a critical role by examining hypothetical scenarios to predict the potential consequences of either implementing or not implementing the proposal [68].

We analyzed the potential impacts of the reconstruction versus non-reconstruction of the BR-319 highway. The climate simulations considered differences in mean fields of 2-meter air temperature, precipitation, evapotranspiration, moisture convergence, and surface runoff during both the wet season (December-January-February, DJF) and dry season (June-July-August, JJA).

3.1. Evaluation of the Eta Regional Climate Model

The performance evaluation of the Eta regional climate model in representing climate patterns was carried out for the year 2021. The evaluated components were air temperature and precipitation. **Figure 4** presents the observed mean air temperature from the SAMeT dataset and the simulated data from the Eta model for the wet (DJF) and dry (JJA) seasons in 2021. In addition, model performance was assessed using bias and Root Mean Square Error (RMSE).

The Eta model successfully reproduced the spatial variability of air temperature across the study area during both wet and dry seasons. When comparing the simulated values to observed data, the mean temperature difference for the wet season (DJF) was 0.003˚C, while for the dry season (JJA) it was −0.29˚C. These differences correspond to 0.01% and −1.08% relative to the observed temperatures for each respective season. Regarding RMSE, lower values were observed during DJF (0.19˚C), whereas greater discrepancies were found during JJA (0.39˚C). Despite these differences, the values were close to the annual mean variation, indicating that the model reasonably captured the seasonal temperature patterns. Therefore, the results suggest that the Eta model was effective in simulating air temperature in the region.

Figure 5 shows the observed precipitation data from CHIRPS and the simulated precipitation fields produced by the Eta regional climate model for the wet season (DJF) and dry season (JJA) of the year 2021. Additionally, bias and root mean square error (RMSE) metrics were calculated to assess model performance.

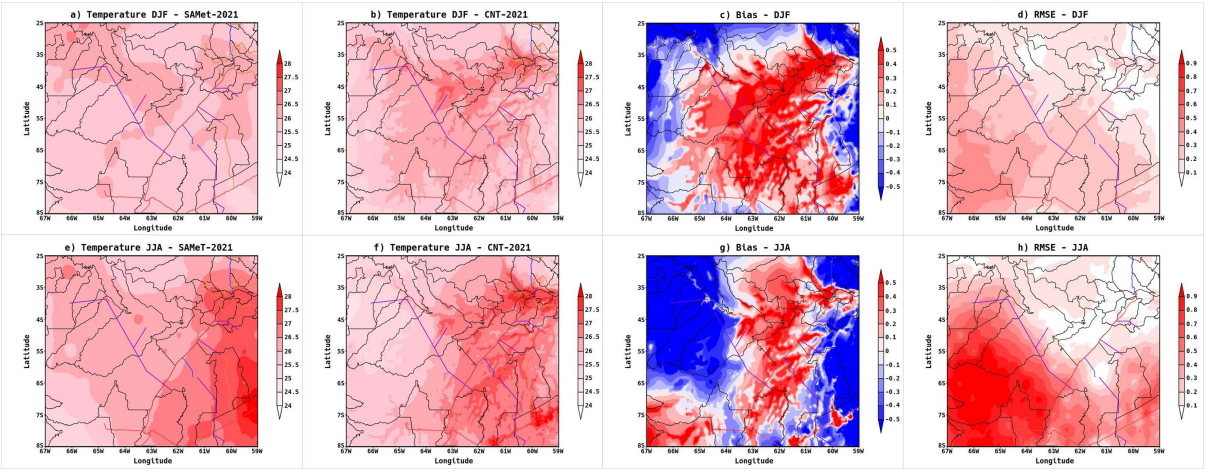

Figure 4. Evaluation of the Eta climate model in representing 2-m air temperature (˚C) for the wet season (DJF): (a) Observed SAMeT 2021, (b) Simulated Eta Model 2021, (c) Bias (˚C), (d) RMSE (˚C); and the dry season (JJA): (e) Observed SAMeT 2021, (f) Simulated Eta Model 2021, (g) Bias (˚C), (h) RMSE (˚C).

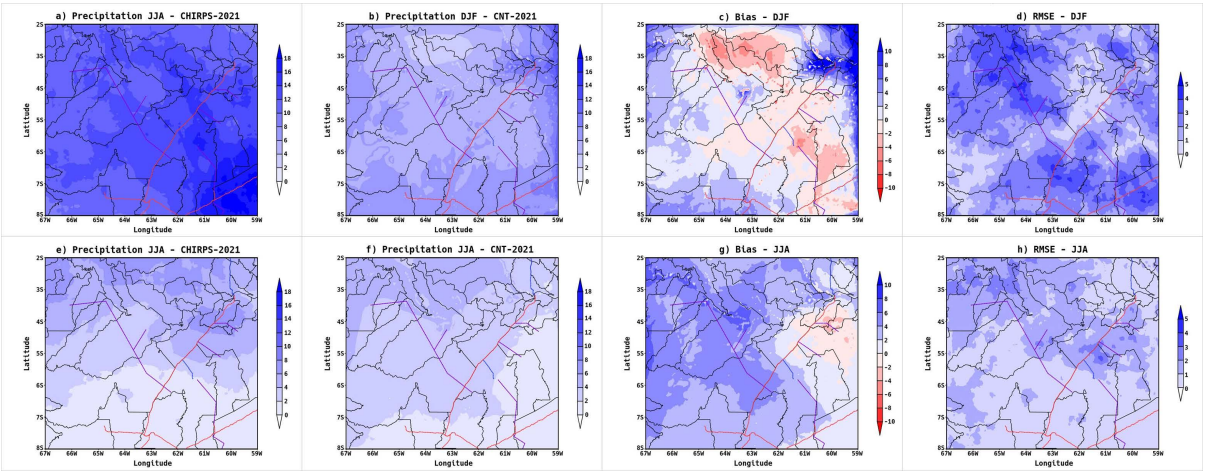

Figure 5. Evaluation of the Eta regional climate model performance in simulating precipitation (mm·day^{-1}) for the wet season (DJF): (a) observed CHIRPS 2021; (b) simulated Eta Model 2021; (c) bias (mm·day^{-1}); (d) RMSE (mm·day^{-1}); and for the dry season (JJA): (e) observed CHIRPS 2021; (f) simulated Eta Model 2021; (g) bias (mm·day^{-1}); (h) RMSE (mm·day^{-1}).

Overall, the Eta model successfully reproduced the spatial variability of precipitation in both seasons across most of the study area. However, it systematically underestimated precipitation values, with an average deviation of −37.5% in DJF and −5.7% in JJA compared to the observed data. This underestimation may be attributed to limitations in the model's physical parameterizations of precipitation or to the numerical integration period, which may have been insufficient for the model to reach dynamic equilibrium. Furthermore, as noted by [69], the Eta model generally tends to underestimate precipitation over large portions of South America.

It should be noted that the Eta model systematically underestimates precipitation, particularly during the wet season (by −37.5%). This bias affects the absolute values of rainfall, but it does not compromise the model's ability to capture spatial

patterns and seasonal contrasts. Consequently, the simulated changes in precipitation across deforestation scenarios should be interpreted as robust in terms of direction and relative magnitude, although the absolute values may be somewhat underestimated.

Regarding the residual error, similar RMSE values were observed for both seasons: 0.17 mm·day^{-1} for DJF and 0.15 mm·day^{-1} for JJA. Despite the underestimation during DJF, the simulated values captured the seasonal variation pattern of annual precipitation. Therefore, the model is considered to have performed satisfactorily in representing precipitation behavior and is suitable for investigating the climate impacts associated with deforestation.

Detailed statistical parameters used for model evaluation (bias and RMSE) are provided in the Supplementary Material (**Appendix B**, **Tables A2-A3**), along with a comparison of the seasonal cycles of observed and simulated air temperature and precipitation (**Appendix B**, **Figure A1**).

3.2. Impact on Air Temperature (2 m)

Figure 6 shows an increase in air temperature during both the wet season (DJF) and the dry season (JJA) when comparing the BAU_1 scenario (unpaved BR-319 highway) and the BAU_2 scenario (paved BR-319 highway) to the current climate baseline (reference year 2021). Relative to the current climate, the BAU_1 scenario projects an average temperature increase of 0.1˚C in both wet and dry seasons by 2050. In the BAU_2 scenario, the average increase by 2050 is 0.1˚C during the wet season and 0.5˚C during the dry season. For the year 2100, the temperature increase reaches 0.3˚C (wet season) and 0.5˚C (dry season) in BAU_1, and 0.4˚C (wet season) and 0.7˚C (dry season) in BAU_2. As illustrated in Figure 6, local temperature increases may exceed 2.5˚C in some deforested regions during the dry season.

The increase in air temperature in deforested areas is related to various factors associated with vegetation removal, particularly changes in surface energy and water balance. Alterations in soil and vegetation parameters, such as porosity, leaf area index, roughness length, and stomatal conductance, modify the surface energy and water flux components, consequently affecting the regional climate in deforested areas. In this study, reduced latent heat flux (evapotranspiration) and increased sensible heat flux over deforested regions contributed to the rise in air temperature, especially during the dry season.

During the wet season, the experiment indicated an increase in latent heat flux and a decrease in sensible heat flux, which acts in the direction opposite to that of the temperature increase. The increase in latent heat flux may have partially mitigated local air warming but did not entirely reverse it. This phenomenon might be linked to changes in surface energy availability. A similar result was reported by [70] in studies on the climatic impacts of deforestation in central Amazonia, which suggested that surface temperature increases, alongside reduced sensible heat flux, can be explained by a reduction in the modeled temperature gradient.

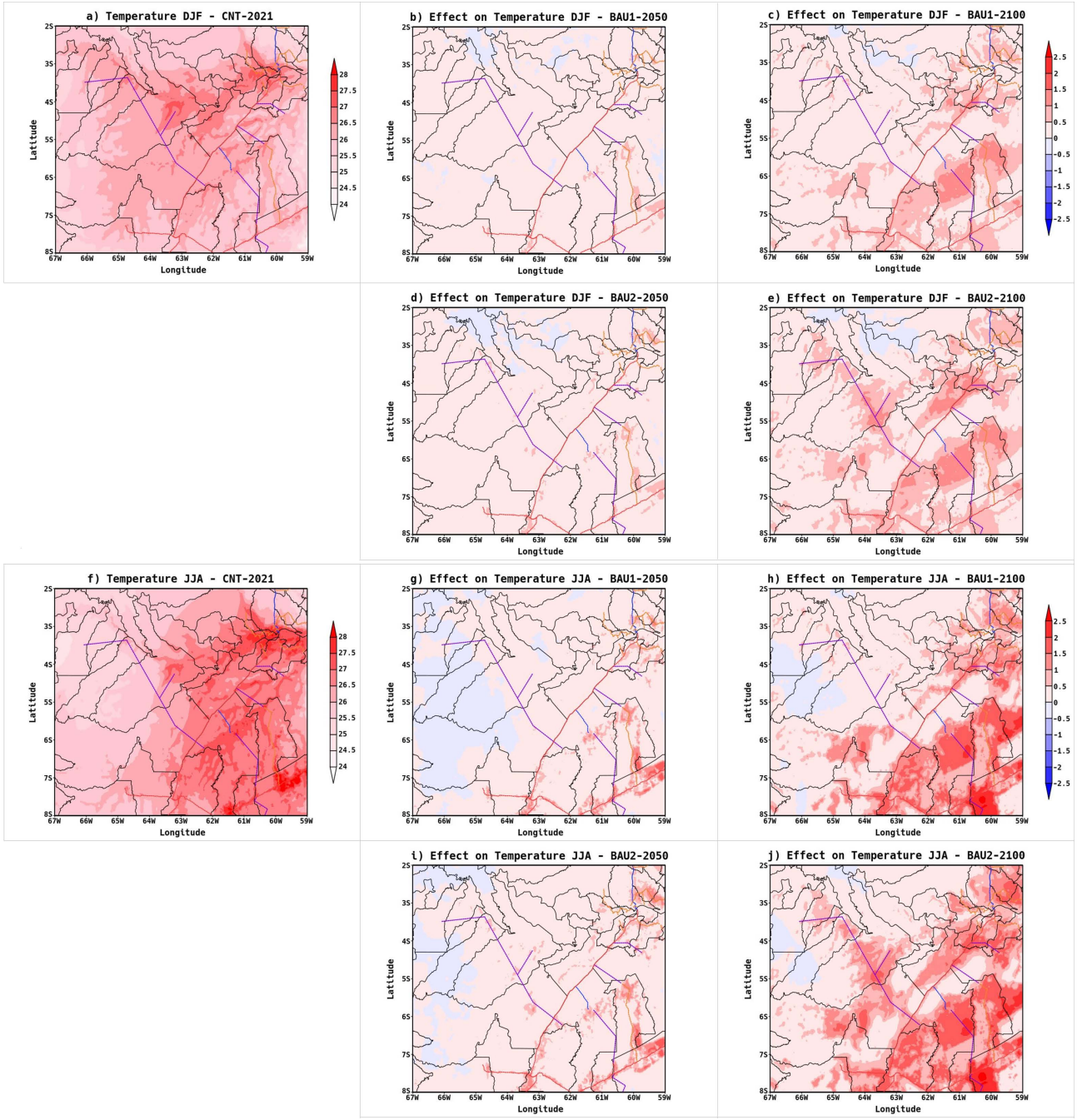

Figure 6. Impact on air temperature (˚C) at 2 m above the ground in 2050 and 2100 resulting from the land-use change scenarios BAU_1 (unpaved BR-319) and BAU_2 (paved BR-319), compared to the current climate (CNT-2021), for the wet season (DJF panels b, c, d, e) and dry season (JJA panels g, h, i, j).

Figure 7 illustrates the impact of paving the BR-319 highway (BAU_2) on air temperature at 2 m, relative to the unpaved scenario (BAU_1). The greatest impact is observed over deforested areas in the northern portion of BR-319 and the central region of the maps, notably around the AM-366 highway, where new deforestation patches are emerging within the forest. Temperature increases are present throughout all analyzed periods, reaching nearly 1.0˚C during the wet season

and 1.5˚C during the dry season in deforested regions.

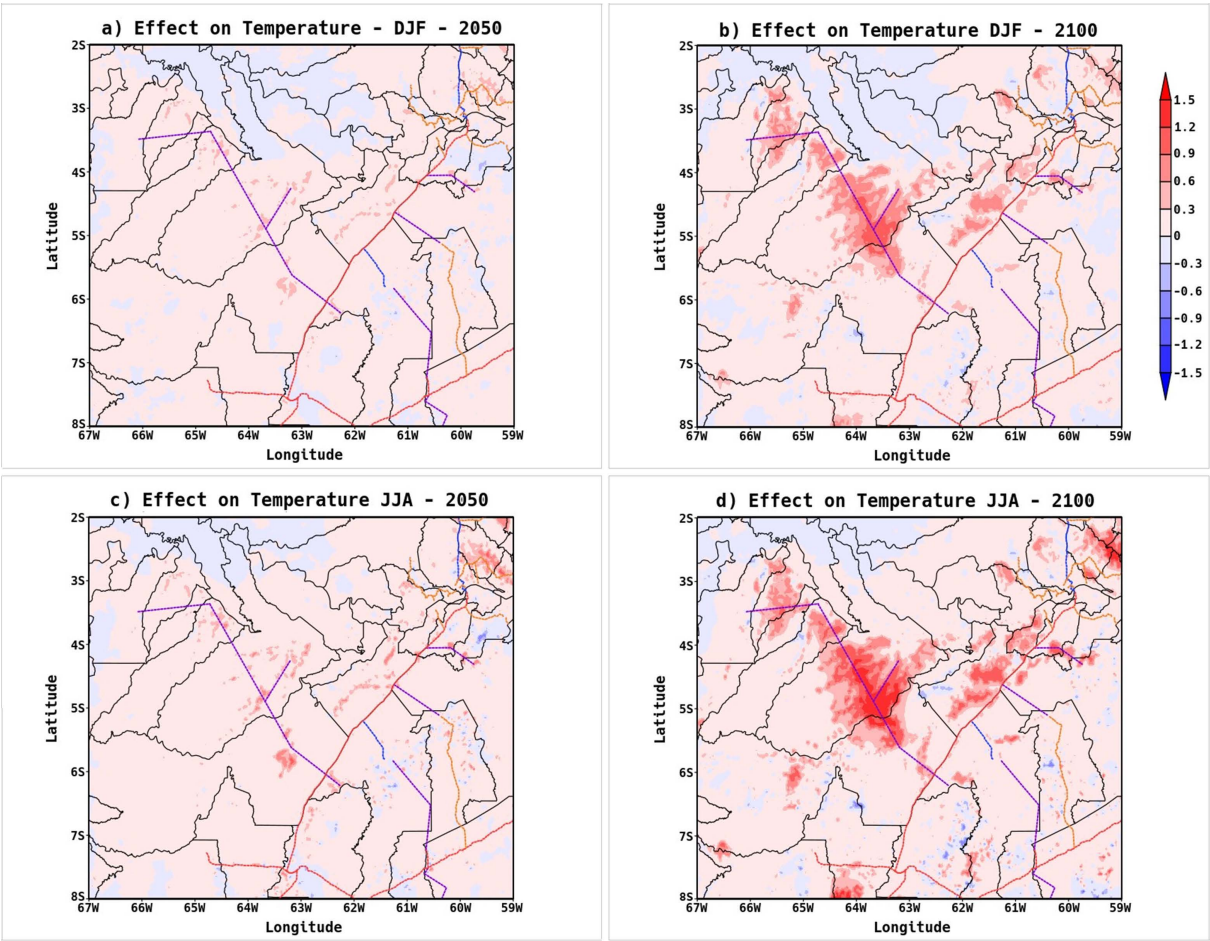

Figure 7. Impact on surface air temperature (˚C) at 2 m above the ground in 2050 and 2100, resulting from the comparison between scenarios BAU_1 (unpaved BR-319 highway) and BAU_2 (paved BR-319 highway), for the wet season (DJF: panels a, d) and dry season (JJA: panels c, d).

A limitation of our approach is that atmospheric CO_2 concentration was held constant in all experiments to isolate the effects of land-use change. However, it is well known that rising CO_2 interacts with vegetation physiology and structure in complex ways. Higher CO_2 concentrations tend to reduce stomatal conductance and evapotranspiration, intensifying regional warming and drying, but may also stimulate biomass growth and leaf area expansion, partly mitigating these impacts [71] [72]. These aspects suggest that the combined effects of land-use change and increasing CO_2 are likely to produce more complex climate responses.

3.3. Impact on Precipitation

Figure 8 presents the impact on precipitation under scenarios BAU_1 and BAU_2 during the wet (DJF) and dry (JJA) seasons for the study area. An increase in precipitation is observed, especially in areas of new "fishbone" deforestation patterns, where deforestation has intensified due to the reconstruction of the BR-319 highway

and the opening of new connecting roads. Comparing the simulated scenarios for 2050 with the current climate, there is an average increase of 0.1 mm·day^{-1} in both the wet and dry seasons for scenarios BAU_1 and BAU_2. By 2100, scenario BAU_1 shows an average increase of 0.4 mm·day^{-1} during the wet season and 0.3 mm·day^{-1} during the dry season, while scenario BAU_2 exhibits an increase of 0.5 mm·day^{-1} and 0.4 mm·day^{-1} for the wet and dry seasons, respectively. As illustrated in **Figure 8**, precipitation increases exceeded 2.5 mm·day^{-1} in some deforested regions. We note that throughout the simulated period the deforestation is in the fishbone pattern, and that, as has occurred on other Amazonian frontiers, it will later be "consolidated" into vast expanses of cleared land. The increase in precipitation in the intermediate deforestation phase represented in the simulation is as expected, but, with progressive consolidation of the deforested landscape, the effect will change to greatly decreased rainfall [73]. The high spatial heterogeneity, here in the form of the "fishbone" pattern, can have an effect at least as important as the area of deforestation in forming the anomalous circulations that led to our simulated precipitation increases during the time span of our study [74]. This effect is temporary, and various conservative assumptions in the deforestation simulation [48] may mean that decreased precipitation begins sooner than the simulated climate implies.

Although it is well established that advancing deforestation results in local warming, impacts on precipitation remain uncertain and continue to be the subject of extensive study [73] [75]. Generally, the literature points to a reduction in precipitation as a consequence of deforestation. However, some studies, such as [18] [28] [30]-[34], report contrasting results. They suggest that in certain areas, precipitation may increase due to forest fragmentation and the dominance of local and mesoscale circulations driven by surface heterogeneity, which is determined by the extent of deforestation. This implies that in areas of smaller-scale deforestation, heterogeneity in sensible and latent heat fluxes can generate intense mesoscale circulations, affecting the planetary boundary layer structure and influencing cloud formation and precipitation patterns [29] [35] [76].

Figure 9 illustrates the impact of paving the BR-319 highway (scenario BAU_2) on precipitation by 2050 and 2100 compared to the unpaved scenario (BAU_1). The greatest impact occurs in the areas influenced by the BR-319 and AM-366 highways, where new deforested areas are opening. The impact intensifies through 2100 in both seasons, with an average increase of 0.1 mm·day^{-1} for the study area. Notably, larger discrepancies are observed during the wet season, with precipitation increases exceeding 1.5 mm·day^{-1} in deforested regions, alongside reductions in precipitation within surrounding forest patches and in areas where deforestation becomes more extensive, particularly in the southeastern portion of the study area.

The results corroborate previously mentioned studies indicating that, as deforestation expands beyond the early "fishbone" phase, an overall decrease in precipitation occurs. The scenario comparisons suggest that increasing deforestation leads to diminished rainfall and heightened regional aridity due to reduced moisture availability and altered atmospheric dynamics.

By 2100, the simulated landscape still represents a transitional stage where both fragmented fishbone deforestation and more consolidated clearings coexist. In areas where deforestation is already extensive, precipitation decreases are evident, whereas in regions with relatively smaller fragments rainfall increases are still observed. It is important to emphasize that 2100 does not represent the endpoint of deforestation in the Amazon, but rather a temporal snapshot under the Business as Usual scenario. As deforestation continues to expand and consolidate beyond 2100, precipitation trends are expected to shift toward significant long-term declines.

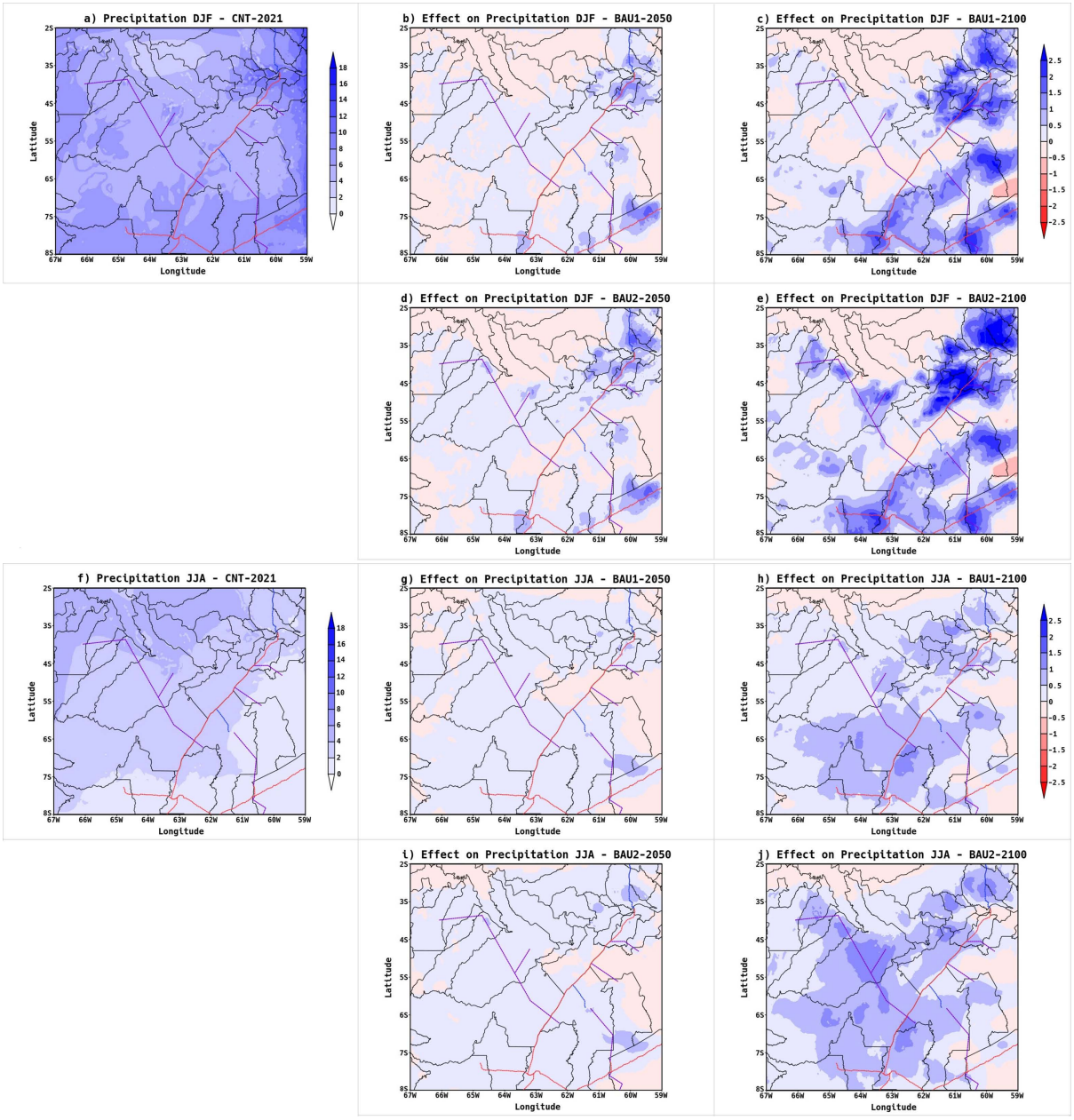

Figure 8. Impact on precipitation (mm·day^{-1}) in 2050 and 2100 resulting from land-use change scenarios BAU_1 (unpaved BR-319 highway) and BAU_2 (paved BR-319 highway), compared to the current climate (CNT-2021), during the wet (DJF) panels b, c, d, e) and dry (JJA) panels g, h, i, j) seasons.

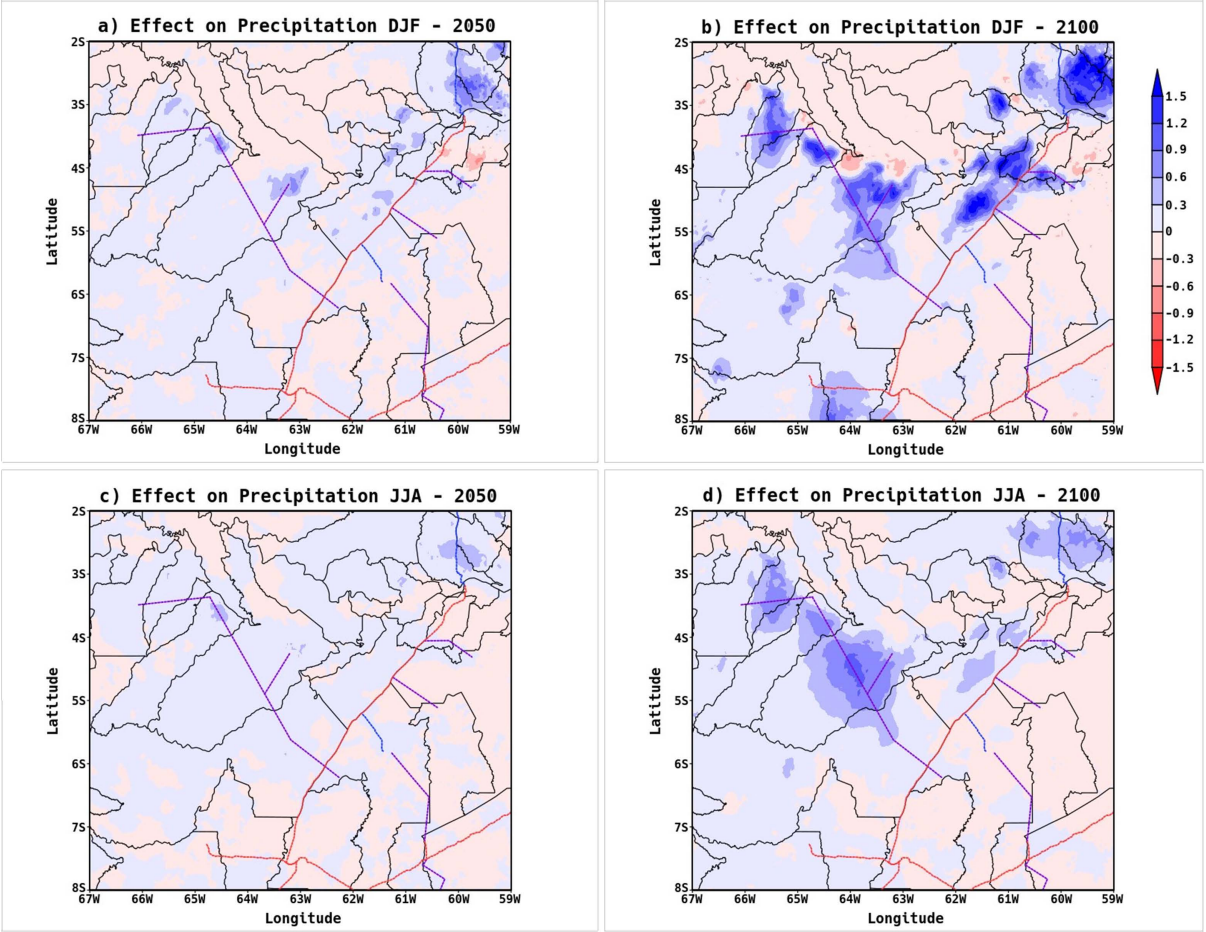

Figure 9. Impact on precipitation (mm·day^{-1}) in 2050 and 2100 resulting from the comparison between scenarios BAU_1 (unpaved BR-319 highway) and BAU_2 (paved BR-319 highway), for the wet (DJF) panels a, d) and dry (JJA) panels c, d) seasons.

3.4. Impact on Evapotranspiration

Figure 10 illustrates the impact of the scenarios on evapotranspiration, showing an increase in evapotranspiration effects in both scenarios during the wet season (DJF), and a reduction during the dry season (JJA). It is evident that during the wet season, evapotranspiration increases, as represented by the rise in latent heat flux.

Evapotranspiration encompasses both soil and surface water evaporation and plant transpiration, which is explained by the increase in latent heat flux. Deforestation reduces transpiration due to the removal of trees and other vegetation that previously performed this function. Consequently, the amount of water vapor released into the atmosphere decreases significantly.

Conversely, results indicate an increase in evapotranspiration during the wet season (DJF), which can be attributed to enhanced local precipitation. This modifies water vapor availability, since forest removal compromises water recycling via evapotranspiration and intensifies direct evaporation from exposed soil surfaces or water bodies. This process may increase local humidity, promote cloud formation, and potentially enhance rainfall occurrence, particularly during wet

periods [77] [78]. Additionally, stomatal resistance is lower in pasture areas than in forests, contributing to increased evaporation in non-forested patches [79].

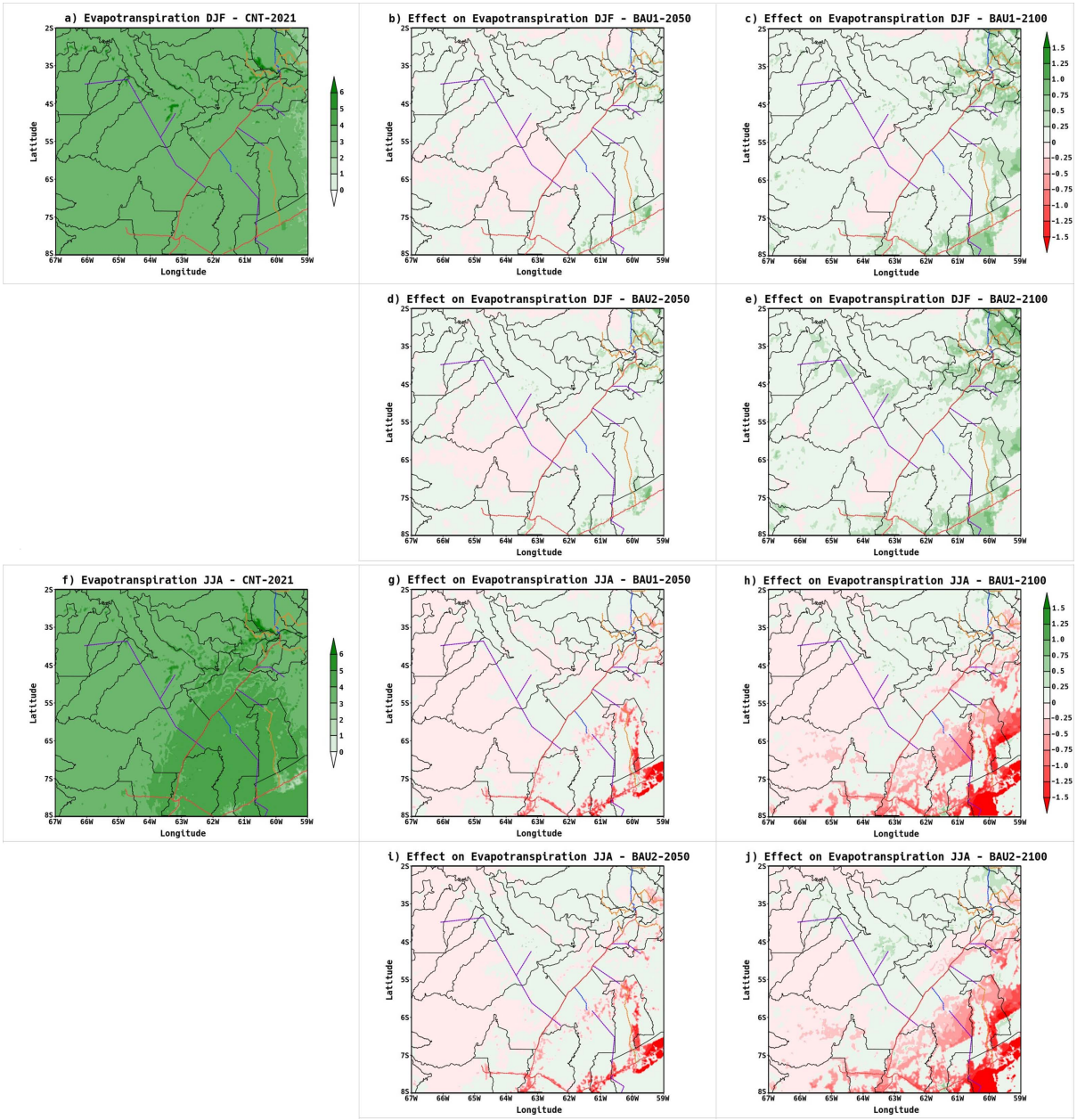

Figure 10. Impact on evapotranspiration (mm·day^{-1}) in 2050 and 2100 resulting from land-use change scenarios BAU_1 (unpaved BR-319 highway) and BAU_2 (paved BR-319 highway), compared to the current climate (CNT-2021), during the wet (DJF) panels b, c, d, e) and dry (JJA) panels g, h, i, j) seasons.

The increase in latent heat flux can also be explained by intensified wind speeds over fragmented areas and the effect of turbulent mixing over wet surfaces in the Amazon [70] [80]. From a micrometeorological perspective, trees at forest edges tend to transpire more than those in the forest interior [81]. This suggests that, at a local scale, forest fragmentation may lead to increased evapotranspiration, par-

tially offsetting reductions caused by deforestation [35].

During the dry season (JJA), evapotranspiration decreases while precipitation increases. This pattern results from mesoscale circulations induced by landscape heterogeneity. According to [31], these processes enhance moisture convergence, which outweighs the reduction in evapotranspiration and consequently increases precipitation.

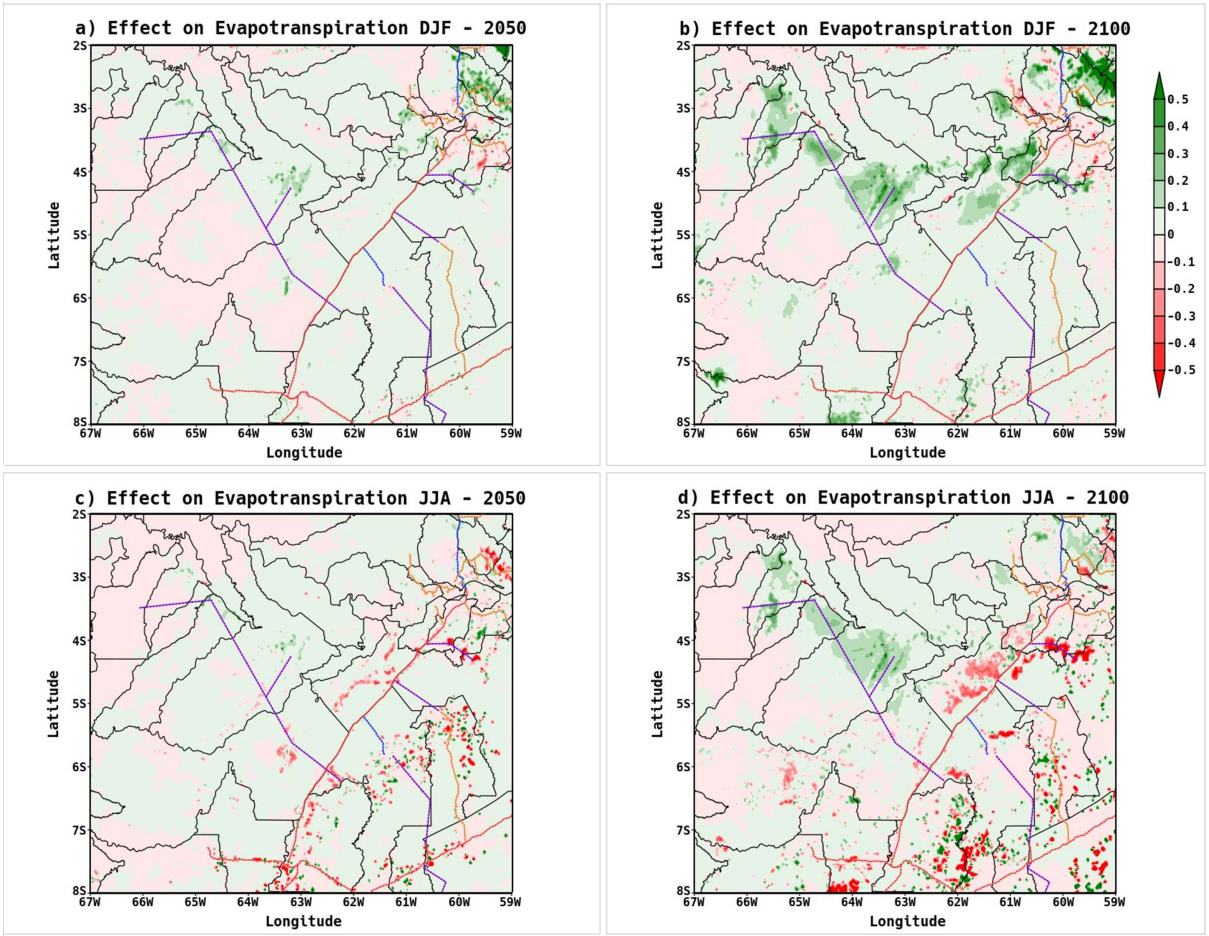

Figure 11. Impact on evapotranspiration (mm·day^{-1}) in 2050 and 2100 resulting from the comparison between scenarios BAU_1 (unpaved BR-319 highway) and BAU_2 (paved BR-319 highway), for the wet (DJF) panels a, d) and dry (JJA) panels c, d) seasons.

Figure 11 depicts the impact of paving the BR-319 highway (scenario BAU_2) on evapotranspiration compared to the unpaved scenario (BAU_1). The most pronounced impact is observed in deforested areas in the northern portion of the BR-319 and central parts of the maps, particularly near the AM-366 highway, where new deforestation patches have formed within the forest matrix. In these deforestation islands influenced by road development, increases in evapotranspiration may exceed 0.5 mm·day^{-1}.

3.5. Impact on Moisture Convergence

Figure 12 shows an increase in moisture convergence within the study area

across all scenarios compared to the control experiment, particularly over newly deforested regions. This result aligns with the previously presented data, indicating that the increase in precipitation is a consequence of enhanced moisture convergence.

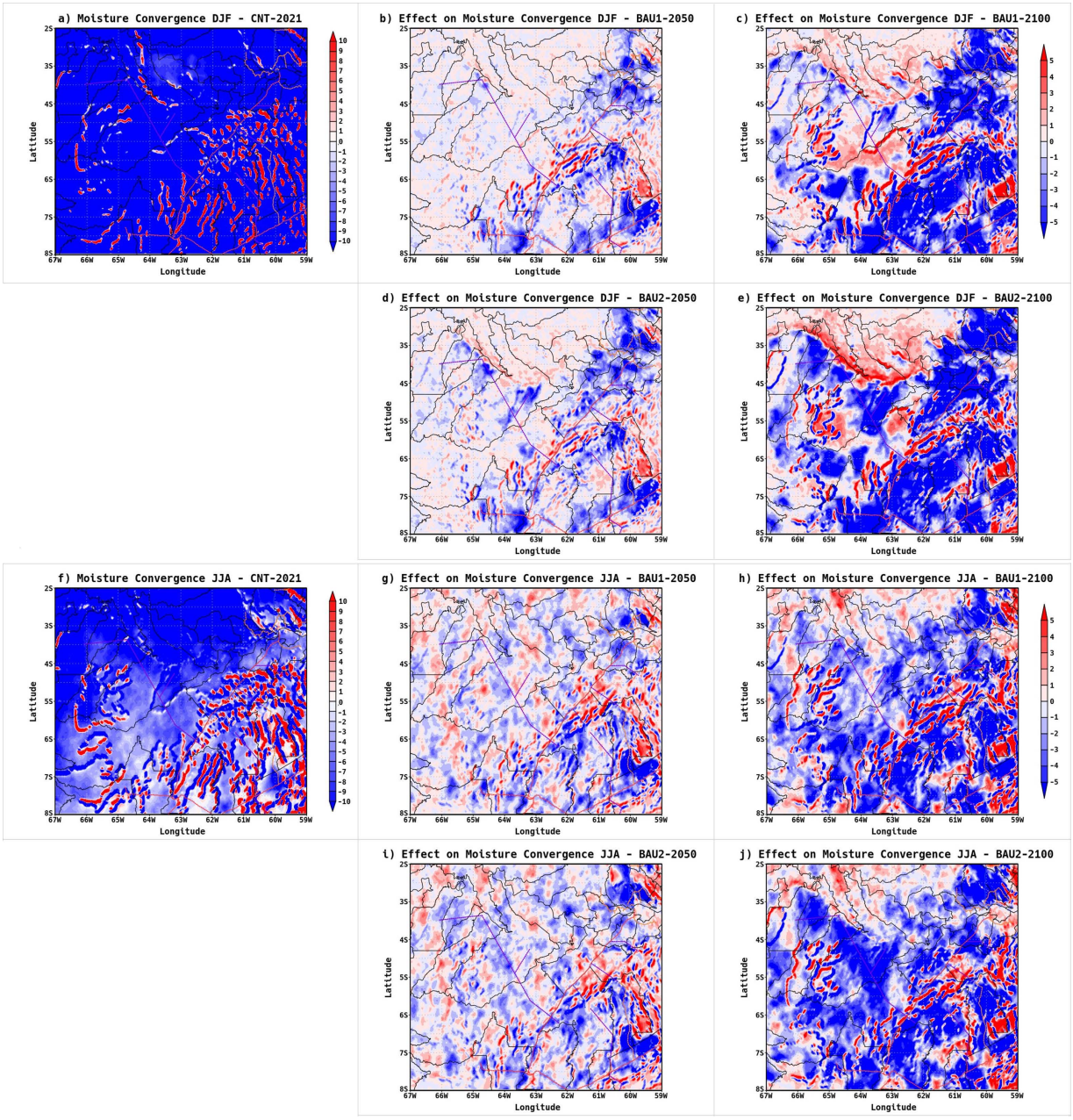

Figure 12. Impact on moisture convergence (mm·day^{-1}) in 2050 and 2100 resulting from land-use change scenarios BAU_1 (unpaved BR-319 highway) and BAU_2 (paved BR-319 highway), compared to the current climate (CNT-2021), during the wet (DJF) panels b, c, d, e) and dry (JJA) panels g, h, i, j) seasons.

It is noteworthy that during the dry season (JJA), the impacts on moisture convergence and evapotranspiration acted in opposite ways. The increase in moisture convergence over deforested areas was sufficiently strong to compensate for the

reduction in evapotranspiration. This rise in precipitation can be explained by changes in local circulation, as alterations in surface heterogeneity due to deforestation generate mesoscale circulations, favoring increased moisture convergence and, consequently, enhanced precipitation over deforested regions [18] [31] [82].

Figure 13 presents the impact on moisture convergence from the comparison between the two analyzed scenarios. The greatest impact is observed along the highways, with a reduction in moisture convergence (positive sign) in the eastern portion of the BR-319 highway and an increase in convergence (negative sign) in deforestation islands, especially considering the opening of new roads such as the AM-366, located more centrally in the maps.

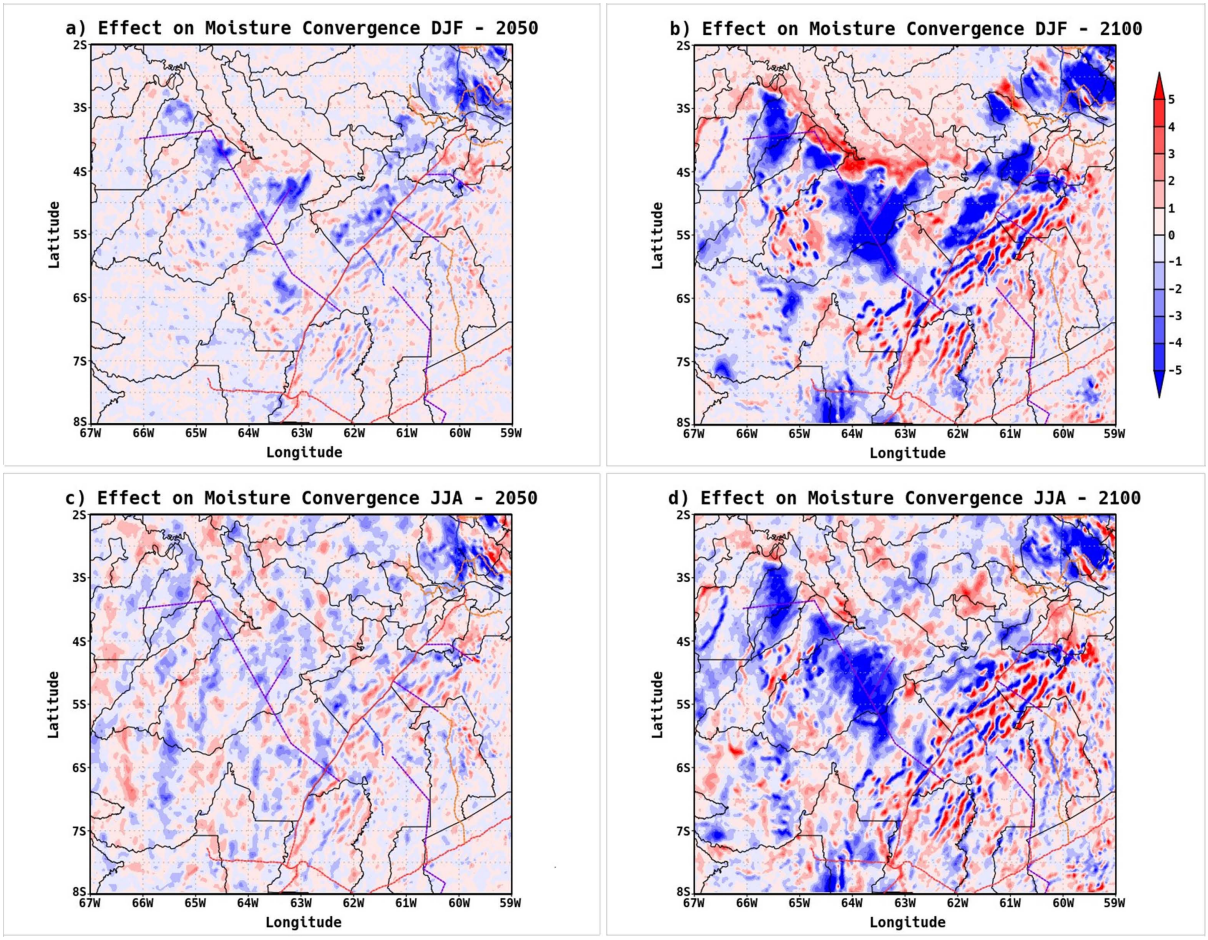

Figure 13. Impact on moisture convergence (mm·day^{-1}) in 2050 and 2100 resulting from the comparison between scenarios BAU_1 (unpaved BR-319 highway) and BAU_2 (paved BR-319 highway), for the wet (DJF) panels a, d) and dry (JJA) panels c, d) seasons.

3.6. Impact on Surface Runoff

Figure 14 presents the mean total runoff simulated by the Eta model for the wet (DJF) and dry (JJA) seasons. During both seasons, runoff values were positive (Precipitation > Evapotranspiration) across most of the study area, with higher

values (>1.5 mm·day^{-1}) observed in deforested areas during the wet season.

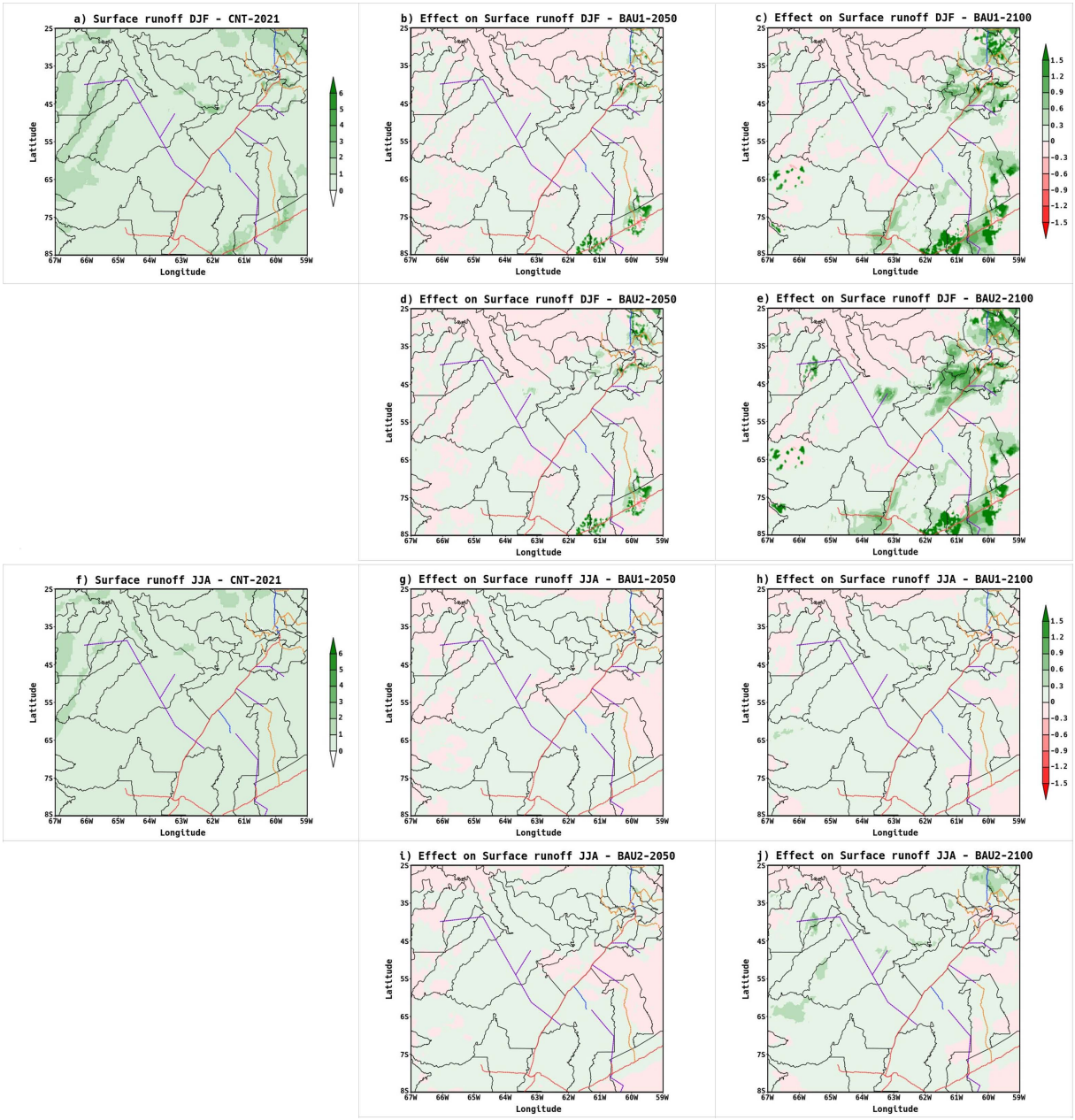

Figure 14. Impact on surface runoff (mm·day^{-1}) in 2050 and 2100 resulting from land-use change scenarios BAU_1 (unpaved BR-319 highway) and BAU_2 (paved BR-319 highway), compared to the current climate (CNT-2021), during the wet (DJF) panels b, c, d, e) and dry (JJA) panels g, h, i, j) seasons.

The increase in surface runoff was primarily driven by the increase in precipitation within the study area. Conventionally, the conversion of forests to agriculture or pasture increases surface runoff partly due to reduced evapotranspiration [83], which was observed during the dry season (JJA) of the experiment. However, during the wet season (DJF), the increased rainfall resulted in a proportional increase in surface runoff. This water availability favored an increase in latent heat

flux, which is responsible for water evaporation, and a reduction in sensible heat flux [84].

Figure 15 shows the impact of paving the BR-319 highway (BAU_2) on surface runoff compared to the unpaved scenario (BAU_1). An average increase in surface runoff of 0.1 mm·day^{-1} was observed across the study area for both seasons until 2100. In some deforested areas, runoff values may exceed 1.0 mm·day^{-1} in both the wet and dry seasons by 2100, following the same pattern observed for precipitation.

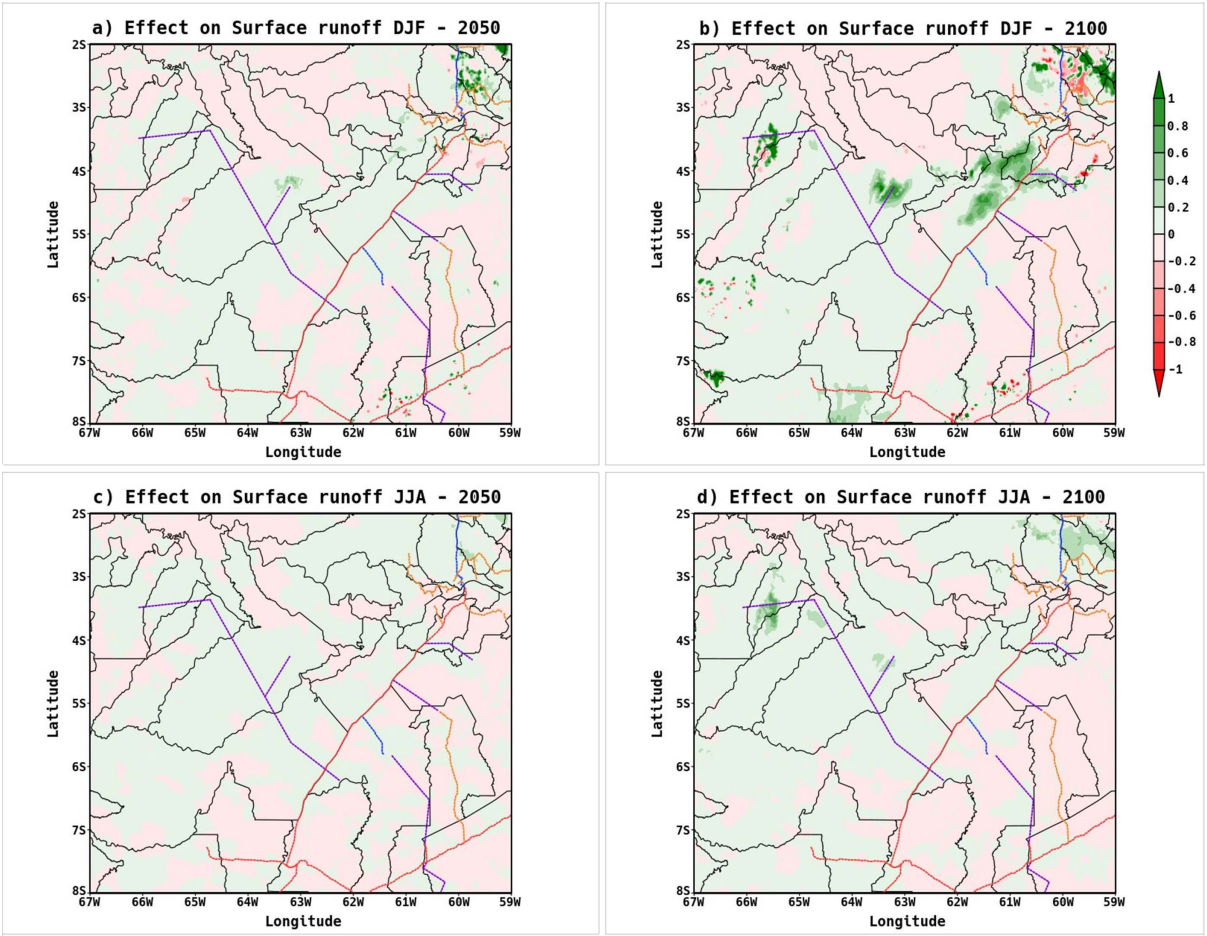

Figure 15. Impact on surface runoff (mm·day^{-1}) in 2050 and 2100 resulting from the comparison between scenarios BAU_1 (unpaved BR-319 highway) and BAU_2 (paved BR-319 highway), for the wet (DJF) panels a, d) and dry (JJA) panels c, d) seasons.

4. Conclusions

Our simulations show a warming signal across all deforestation scenarios, with the most intense response associated with the paving of the BR-319 highway by the end of the century, particularly during the dry season, when mean air temperature increases approach 0.7˚C. At the local scale, deforested areas exhibit stronger anomalies, in some cases exceeding 2.5˚C.

Changes in precipitation also occur: on average, increases of about 0.5

mm·day^{-1} were simulated across the study area, with local increments above 2.5 mm·day^{-1}. These effects are linked to changes in local circulation, as surface heterogeneity induced by deforestation favors mesoscale processes that enhance regional moisture convergence. However, this effect is transitional and tends to shift toward rainfall decline as deforestation consolidates into large continuous clearings.

Warming over deforested areas results from alterations in the surface energy and water balance. Although an increase in latent heat flux may exert a localized cooling effect, it is outweighed by the overall warming induced by forest loss. Our results also indicate that intensified deforestation contributes to the drying of adjacent forests and exacerbates existing climatic challenges in the Amazon, such as rising temperatures and the intensification of dry seasons.

These findings provide important insights for decision-making on road infrastructure projects in the Amazon, such as BR-319 and AM-366. The climatic consequences of large-scale road development need to be considered in the planning and approval processes for such projects.

Based on our results, we recommend the incorporation of high-resolution regional climate modeling into Strategic Environmental Assessments (SEAs) of governmental Policies, Plans, and Programs (PPPs) for road infrastructure projects in the Amazon. This approach is essential to assess the local impacts of road expansion on deforestation and to ensure that public policy decisions are guided by the best available scientific evidence.

Acknowledgements

This study was developed in the Postgraduate Program in Climate and Environment (CLIAMB) jointly coordinated by the Amazon State University (UEA) and the National Institute of Research in Amazonia (INPA). All authors thank the Center for Weather Forecasting and Climate Studies at the National Institute of Space Research (CPTEC/INPE) for making available the numerical integrations datasets, the National Center for High Performance Processing (CENAPAD/UNICAMP) and the Laboratory of Terrestrial Climate Systems Modeling Laboratory (LABCLIM/UEA) for providing the computational infrastructure (TAMBAQUI Cluster). The Amazonas State Research Support Foundation (FAPEAM) (Resolution 003/2019; 01.02.016301.02529/2024-87) and the Coordination for the Improvement of Higher Education Personnel (CAPES) (Finance Code 001), for institutional support. The first author thanks the Brazilian Institute of the Environment and Renewable Natural Resources (IBAMA) for its support. We thank the National Council for Scientific and Technological Development (CNPq 312450/2021-4; 406941/2022-0), and the Brazilian Research Network on Climate Change (Rede Clima) (FINEP/Rede Clima 01.13.0353-00.

Conflicts of Interest

The authors declare no conflicts of interest regarding the publication of this paper.

References

[1] Nobre, C.A., Sampaio, G., Borma, L.S., Castilla-Rubio, J.C., Silva, J.S. and Cardoso, M. (2016) Land-Use and Climate Change Risks in the Amazon and the Need of a Novel Sustainable Development Paradigm. *Proceedings of the National Academy of Sciences*, **113**, 10759-10768. https://doi.org/10.1073/pnas.1605516113

[2] Marengo, J.A. and Nobre, C.A. (2009) Clima da região amazônica. In: Cavalcanti, I.F.A., Ferreira, N.J., da Silva, M.G.A.J. and Silva Dias, M.A.F., Eds., *Tempo e Clima no Brasil*, Oficina de Textos, 197-212. https://www.researchgate.net/publication/329466396_Mudancas_Climaticas_impactos_e_cenarios_para_a_Amazonia

[3] Nobre, C.A., Marengo, J.A. and Artaxo, P. (2009) Understanding the Climate of Amazonia: Progress from LBA. In: Keller, M., *et al.*, Eds., *Amazonia and Global Change*, American Geophysical Union, 145-147. https://doi.org/10.1029/2009gm000903

[4] Zemp, D.C., Schleussner, C., Barbosa, H.M.J., Hirota, M., Montade, V., Sampaio, G., *et al.* (2017) Self-Amplified Amazon Forest Loss Due to Vegetation-Atmosphere Feedbacks. *Nature Communications*, **8**, Article No. 14681. https://doi.org/10.1038/ncomms14681

[5] Fearnside, P.M., Barbosa, R.I. and Pereira, V.B. (2013) Emissões de gases do efeito estufa por desmatamento e incêndios florestais em Roraima: Fontes e sumidouros. *Revista Agro@mbiente On-Line*, **7**, 95-111. https://doi.org/10.18227/1982-8470ragro.v7i1.971

[6] Rocha, V.M., Correia, F.W.S., Satyamurty, P., De Freitas, S.R., Moreira, D.S., Da Silva, P.R.T., *et al.* (2015) Impacts of Land Cover and Greenhouse Gas (GHG) Concentration Changes on the Hydrological Cycle in Amazon Basin: A Regional Climate Model Study. *Revista Brasileira de Climatologia*, **15**, 7-27. https://doi.org/10.5380/abclima.v15i0.36386

[7] Marengo, J.A., Souza, C.M., Thonicke, K., Burton, C., Halladay, K., Betts, R.A., *et al.* (2018) Changes in Climate and Land Use over the Amazon Region: Current and Future Variability and Trends. *Frontiers in Earth Science*, **6**, Article No. 228. https://doi.org/10.3389/feart.2018.00228

[8] Weng, W., Luedeke, M.K.B., Zemp, D.C., Lakes, T. and Kropp, J.P. (2018) Aerial and Surface Rivers: Downwind Impacts on Water Availability from Land Use Changes in Amazonia. *Hydrology and Earth System Sciences*, **22**, 911-927. https://doi.org/10.5194/hess-22-911-2018

[9] Marengo, J.A. and Souza-Jr., C.M. (2018) Mudanças Climáticas: Impactos e cenários para an Amazônia. PPG em Ciência Ambiental-USP. https://www.oamanhaehoje.com.br/assets/pdf/Relatorio_Mudancas_Climaticas-Amazonia.pdf

[10] Fearnside, P.M. (2020) Uso da terra na Amazônia e as mudanças climáticas globais. In: Fearnside, P.M., Ed., *Destruição e Conservação da Floresta Amazônica*, Vol. 1, Editora do INPA, 21-38. https://www.researchgate.net/publication/340923492_Uso_da_terra_na_Amazonia_e_as_mudancas_climaticas_globais

[11] Pielke, R.A., Pitman, A., Niyogi, D., Mahmood, R., McAlpine, C., Hossain, F., *et al.* (2011) Land Use/Land Cover Changes and Climate: Modeling Analysis and Observational Evidence. *WIREs Climate Change*, **2**, 828-850. https://doi.org/10.1002/wcc.144

[12] Gash, J.H.C. and Nobre, C.A. (1997) Climatic Effects of Amazonian Deforestation:

Some Results from ABRACOS. *Bulletin of the American Meteorological Society*, **78**, 823-830. https://doi.org/10.1175/1520-0477(1997)078<0823:ceoads>2.0.co;2

[13] Marengo, J.A. and Espinoza, J.C. (2015) Extreme Seasonal Droughts and Floods in Amazonia: Causes, Trends and Impacts. *International Journal of Climatology*, **36**, 1033-1050. https://doi.org/10.1002/joc.4420

[14] Seymour, F., Wolosin, M. and Gray, E. (2022) Not Just Carbon: Capturing All the Benefits of Forests for Stabilizing the Climate from Local to Global Scales. Report, World Resources Institute. https://doi.org/10.46830/wrirpt.19.00004

[15] Gerow, A. and Seymour, F. (2023) Resumo Para Gestores de Política Implicações para o setor privado sobre os efeitos do desmatamento de florestas tropicais para além do carbono. https://files.wri.org/d8/s3fs-public/2023-09/implicacoes-para-o-setor-privado.pdf

[16] Guimberteau, M., Ciais, P., Ducharne, A., Boisier, J.P., Dutra Aguiar, A.P., Biemans, H., *et al.* (2017) Impacts of Future Deforestation and Climate Change on the Hydrology of the Amazon Basin: A Multi-Model Analysis with a New Set of Land-Cover Change Scenarios. *Hydrology and Earth System Sciences*, **21**, 1455-1475. https://doi.org/10.5194/hess-21-1455-2017

[17] Gomes, W.d.B., Correia, F.W.S., Capistrano, V., Veiga, J.A.P., Vergasta, L.A., Chou, S.C., *et al.* (2020) Avaliação dos Impactos das Mudanças na Cobertura da Terra e Cenário de Emissões (RCP 8.5) no Balanço de água na Bacia do Rio Madeira. *Revista Brasileira de Meteorologia*, **35**, 689-702. https://doi.org/10.1590/0102-77863540076

[18] Qin, Y., Wang, D., Ziegler, A.D., Fu, B. and Zeng, Z. (2025) Impact of Amazonian Deforestation on Precipitation Reverses between Seasons. *Nature*, **639**, 102-108. https://doi.org/10.1038/s41586-024-08570-y

[19] Yoon, A. and Hohenegger, C. (2025) Muted Amazon Rainfall Response to Deforestation in a Global Storm-Resolving Model. *Geophysical Research Letters*, **52**, e2024GL110503. https://doi.org/10.1029/2024gl110503

[20] Lyra, A., Chou, S.C. and Dereczynski, C.P. (2007) Indicadores de turbulência a partir de previsões do modelo regional Eta. *Revista Brasileira de Meteorologia*, **22**, 160-181. https://oasisbr.ibict.br/vufind/Record/SBMET-1_e6cf9131a1b15ce00782d3715d01ab77

[21] Chou, S.C., Nobre, P., Maia, A., Freitas, E.D., Sampaio, G., Cavalcanti, I.F.A., *et al.* (2014) Avaliação de modelos globais e regionais climáticos. In: *Base Científica das Mudanças Climáticas*: *V*1—*Primeiro Relatório da Avaliação Nacional*, UFRJ/PBMC, 323-361. http://mtc-m16d.sid.inpe.br/col/sid.inpe.br/mtc-m19/2012/01.04.16.25/doc/PBMC-VOLUME1-RAN1_8.pdf

[22] Feser, F., Rockel, B., von Storch, H., Winterfeldt, J. and Zahn, M. (2011) Regional Climate Models Add Value to Global Model Data: A Review and Selected Examples. *Bulletin of the American Meteorological Society*, **92**, 1181-1192. https://doi.org/10.1175/2011bams3061.1

[23] Rockel, B. (2015) The Regional Downscaling Approach: A Brief History and Recent Advances. *Current Climate Change Reports*, **1**, 22-29. https://doi.org/10.1007/s40641-014-0001-3

[24] Ambrizzi, T., Reboita, M.S., da Rocha, R.P. and Llopart, M. (2018) The State of the Art and Fundamental Aspects of Regional Climate Modeling in South America. *Annals of the New York Academy of Sciences*, **1436**, 98-120. https://doi.org/10.1111/nyas.13932

[25] Goddard, L., Mason, S.J., Zebiak, S.E., Ropelewski, C.F., Basher, R. and Cane, M.A.

(2001) Current Approaches to Seasonal to Interannual Climate Predictions. *International Journal of Climatology*, **21**, 1111-1152. https://doi.org/10.1002/joc.636

[26] Chou, S.C., Marengo, J.A., Lyra, A.A., Sueiro, G., Pesquero, J.F., Alves, L.M., *et al.* (2011) Downscaling of South America Present Climate Driven by 4-Member HadCM3 Runs. *Climate Dynamics*, **38**, 635-653. https://doi.org/10.1007/s00382-011-1002-8

[27] Avissar, R., Silva Dias, P.L., Silva Dias, M.A.F. and Nobre, C. (2002) The Large-Scale Biosphere-Atmosphere Experiment in Amazonia (LBA): Insights and Future Research Needs. *Journal of Geophysical Research*: *Atmospheres*, **107**, Article No. 8086. https://doi.org/10.1029/2002jd002704

[28] Werth, D. and Avissar, R. (2002) The Local and Global Effects of Amazon Deforestation. *Journal of Geophysical Research*: *Atmospheres*, **107**, Article No. 8087. https://doi.org/10.1029/2001jd000717

[29] Baidya Roy, S. and Avissar, R. (2002) Impact of Land Use/Land Cover Change on Regional Hydrometeorology in Amazonia. *Journal of Geophysical Research*: *Atmospheres*, **107**, Article No. 8037. https://doi.org/10.1029/2000jd000266

[30] Correia, F., Alvalá, R. and Manzi, A. (2006) Impacto das modificações da cobertura vegetal no balanço de água na Amazônia: Um estudo com modelo de circulação geral da atmosfera (MCGA). *Revista Brasileira de Meteorologia*, **21**, 153-167. http://mtc-m16b.sid.inpe.br/col/sid.inpe.br/mtc-m17@80/2007/04.23.18.44/doc/correia_rbm.pdf

[31] Correia, F.W.S., Manzi, A.O., Cândido, L.A., Santos, R.M.N. and Pauliquevis, T. (2007) Balanço de umidade na Amazônia e sua sensibilidade às mudanças na cobertura vegetal. *Ciência e Cultura*, **59**, 39-43. http://cienciaecultura.bvs.br/pdf/cic/v59n3/a16v59n3.pdf

[32] Correia, F.W.S., Alvalá, R.C.S. and Manzi, A.O. (2007) Modeling the Impacts of Land Cover Change in Amazonia: A Regional Climate Model (RCM) Simulation Study. *Theoretical and Applied Climatology*, **93**, 225-244. https://doi.org/10.1007/s00704-007-0335-z

[33] Pitman, A.J. and Lorenz, R. (2016) Scale Dependence of the Simulated Impact of Amazonian Deforestation on Regional Climate. *Environmental Research Letters*, **11**, Article ID: 094025. https://doi.org/10.1088/1748-9326/11/9/094025

[34] Chambers, J.Q. and Artaxo, P. (2017) Deforestation Size Influences Rainfall. *Nature Climate Change*, **7**, 175-176. https://doi.org/10.1038/nclimate3238

[35] Spracklen, D.V., Baker, J.C.A., Garcia-Carreras, L. and Marsham, J.H. (2018) The Effects of Tropical Vegetation on Rainfall. *Annual Review of Environment and Resources*, **43**, 193-218. https://doi.org/10.1146/annurev-environ-102017-030136

[36] Fearnside, P.M., Graça, P.M.L.d.A., Keizer, E.W.H., Maldonado, F.D., Barbosa, R.I. and Nogueira, E.M. (2009) Modelagem de desmatamento e emissões de gases de efeito estufa na região sob influência da rodovia Manaus-Porto Velho (BR-319). *Revista Brasileira de Meteorologia*, **24**, 208-233. https://doi.org/10.1590/s0102-77862009000200009

[37] Fearnside, P.M. and Graça, P.M.L.d.A. (2009) BR-319: A rodovia Manaus-Porto Velho e o impacto potencial de conectar o arco de desmatamento à Amazônia central. *Novos Cadernos NAEA*, **12**, 19-50. https://doi.org/10.5801/ncn.v12i1.241

[38] Andrade, M.B., Ferrante, L. and Fearnside, P.M. (2021) Brazil's Highway BR-319 Demonstrates a Crucial Lack of Environmental Governance in Amazonia. *Environmental Conservation*, **48**, 161-164. https://doi.org/10.1017/s0376892921000084

[39] Ferrante, L., Andrade, M.B.T. and Fearnside, P.M. (2021) Land Grabbing on Brazil's

Highway BR-319 as a Spearhead for Amazonian Deforestation. *Land Use Policy*, **108**, Article ID: 105559. https://doi.org/10.1016/j.landusepol.2021.105559

[40] Fearnside, P.M. (2024) Impactos da rodovia BR-319-9: O discurso de governança. Amazônia Real, 26 June 2024. https://amazoniareal.com.br/impactos-da-rodovia-br-319-9-o-discurso-de-governanca/

[41] Fearnside, P.M. (2024) O relatório do GT BR-319 de DNIT: A mais recente manobra para obter aprovação para um desastre ambiental. Amazônia Real, 13 June 2024. https://amazoniareal.com.br/o-relatorio-do-gt-br-319-de-dnit-a-mais-recente-manobra-para-obter-aprovacao-para-um-desastre-ambiental/

[42] De Castro, E.M.R., Monteiro, R. and Castro, C.P. (2004) Dinâmica de atores, uso da terra e desmatamento na rodovia Cuiabá-Santarém (Paper 179). *Papers do NAEA*, **1**, 1-67. https://doi.org/10.18542/papersnaea.v13i1.11558

[43] Passos, M.M. (2017) BR-163, de Cuiabá a Santarém: O papel dos agentes e sujeitos no ordenamento do território e na implementação de políticas públicas. *Ci. & Tróp. Recife*, **41**, 139-164. https://periodicos.fundaj.gov.br/CIC/article/view/1609/1334

[44] Brito, R. and Castro, E. (2018) Development and Conflict in the Amazon—A Glimpse into the Coloniality of On-Going Processes in Br-163. *Revista NERA*, **42**, 51-73. https://doi.org/10.47946/rnera.v0i42.5679

[45] INPE—Instituto Nacional de Pesquisas Espaciais (2023) PRODES. http://terrabrasilis.dpi.inpe.br/app/dashboard/deforestation/biomes/legal_amazon/rates

[46] Barni, P.E., Fearnside, P.M. and Graça, P.M.L.A. (2018) Simulando desmatamento e perda de carbono na Amazônia: Impactos no Estado de Roraima devido à reconstrução da BR-319 (Manaus-Porto Velho). In: Oliveira, S.K.S. and Falcão, M.T., Eds., *Roraima*: *Biodiversidade e Diversidades*, Editora da Universidade Estadual de Roraima (UERR), 154-173. https://repositorio.inpa.gov.br/handle/1/35364

[47] Fearnside, P.M. (2018) BR-319 e a destruição da floresta amazônica. Amazônia Real 19 October 2018. https://amazoniareal.com.br/br-319-e-destruicao-da-floresta-amazonica/

[48] Santos, J.L., Yanai, A.M., Graça, P.M.L.A., Correia, F.W.S. and Fearnside, P.M. (2023) Amazon Deforestation: Simulated Impact of Brazil's Proposed BR-319 Highway Project. *Environmental Monitoring and Assessment*, **195**, Article No. 1217. https://doi.org/10.1007/s10661-023-11820-7

[49] Laurance, W.F., Cochrane, M.A., Bergen, S., Fearnside, P.M., Delamônica, P., Barber, C., *et al.* (2001) The Future of the Brazilian Amazon. *Science*, **291**, 438-439. https://doi.org/10.1126/science.291.5503.438

[50] Laurance, W.F., Clements, G.R., Sloan, S., O'Connell, C.S., Mueller, N.D., Goosem, M., *et al.* (2014) A Global Strategy for Road Building. *Nature*, **513**, 229-232. https://doi.org/10.1038/nature13717

[51] Barber, C.P., Cochrane, M.A., Souza, C.M. and Laurance, W.F. (2014) Roads, Deforestation, and the Mitigating Effect of Protected Areas in the Amazon. *Biological Conservation*, **177**, 203-209. https://doi.org/10.1016/j.biocon.2014.07.004

[52] Ferrante, L. and Fearnside, P.M. (2019) Brazil's New President and "Ruralists" Threaten Amazonia's Environment, Traditional Peoples and the Global Climate. *Environmental Conservation*, **46**, 261-263. https://doi.org/10.1017/s0376892919000213

[53] Fearnside, P.M., Ferrante, L., Yanai, A.M. and Isaac-Júnior, M.A. (2020) Trans-Purus: Brazil's Last Intact Amazon Forest at Immediate Risk (Commentary). Monga-

bay.
https://news.mongabay.com/2020/11/trans-purus-brazils-last-intact-amazon-forest-at-immediate-risk-commentary/

[54] IBGE—Instituto Brasileiro de Geografia e Estatística (2017) Geociências.
https://www.ibge.gov.br/geociencias/downloads-geociencias.html

[55] ICMBio—Instituto Chico Mendes de Conservação da Biodiversidade (2019) Limites das Unidades de Conservação Federais (atualizado em julho de 2019): Unidades de Conservação Federais—SHP (SIRGAS2000).
https://www.gov.br/icmbio/pt-br/assuntos/dados_geoespaciais/mapa-tematico-e-dados-geoestatisticos-das-unidades-de-conservacao-federais

[56] INCRA—Instituto Nacional de Colonização e Reforma Agrária (s.d.).
https://dados.gov.br/dados/conjuntos-dados/acervo-fundiario

[57] FUNAI (Fundação Nacional do Índio) (n.d.) Download de dados geográficos: Terra Indígena (Regularizada, Homologada, Declarada, Delimitada e Área em Estudo).
https://www.gov.br/funai/pt-br/atuacao/terras-indigenas/geoprocessamento-e-mapas

[58] Alvares, C.A., Stape, J.L., Sentelhas, P.C., de Moraes Gonçalves, J.L. and Sparovek, G. (2013) Köppen's Climate Classification Map for Brazil. *Meteorologische Zeitschrift*, **22**, 711-728. https://doi.org/10.1127/0941-2948/2013/0507

[59] Fisch, G., Marengo, J.A. and Nobre, C.A. (1996) Clima da Amazônia. Revista Climanálise.
https://www.ecodebate.com.br/2014/11/13/clima-da-amazonia-por-gilberto-fisch-jose-a-marengo-e-carlos-a-nobre/

[60] Leite-Filho, A.T., Soares-Filho, B.S., Davis, J.L. and Rodrigues, H.O. (2020) Modeling Environmental Dynamics with Dinamica EGO.
https://www.csr.ufmg.br/dinamica/dokuwiki/doku.php?id=guidebook_start

[61] Chou, S.C., Bustamante, J.F. and Gomes, J.L. (2005) Evaluation of Eta Model Seasonal Precipitation Forecasts over South America. *Nonlinear Processes in Geophysics*, **12**, 537-555. https://doi.org/10.5194/npg-12-537-2005

[62] Mesinger, F., Janjić, Z.I., Ničković, S., Gavrilov, D. and Deaven, D.G. (1988) The Step-Mountain Coordinate: Model Description and Performance for Cases of Alpine Lee Cyclogenesis and for a Case of an Appalachian Redevelopment. *Monthly Weather Review*, **116**, 1493-1518.
https://doi.org/10.1175/1520-0493(1988)116<1493:tsmcmd>2.0.co;2

[63] Janjić, Z.I. (1994) The Step-Mountain Eta Coordinate Model: Further Developments of the Convection, Viscous Sublayer, and Turbulence Closure Schemes. *Monthly Weather Review*, **122**, 927-945.
https://doi.org/10.1175/1520-0493(1994)122<0927:tsmecm>2.0.co;2

[64] Chou, S.C. (1996) Modelo regional Eta. Climanálise, Edição Comemorativa de 10 anos. Centro de Previsão de Tempo e Estudos Climáticos (CPTEC).
http://climanalise.cptec.inpe.br/~rclimanl/especial.html

[65] Harrigan, S., Zsoter, E., Alfieri, L., Prudhomme, C., Salamon, P., Wetterhall, F., *et al.* (2020) GloFAS-ERA5 Operational Global River Discharge Reanalysis 1979-Present. *Earth System Science Data*, **12**, 2043-2060.
https://doi.org/10.5194/essd-12-2043-2020

[66] Funk, C., Peterson, P., Landsfeld, M., Pedreros, D., Verdin, J., Shukla, S., *et al.* (2015) The Climate Hazards Infrared Precipitation with Stations—A New Environmental Record for Monitoring Extremes. *Scientific Data*, **2**, Article ID: 150066.
https://doi.org/10.1038/sdata.2015.66

[67] INPE—Instituto Nacional de Pesquisas Espaciais (2024) Dados SAMeT. http://ftp.cptec.inpe.br/modelos/tempo/SAMeT/Read-me.pdf

[68] Sánchez, L.E. (2013) Avaliação de Impacto Ambiental: Conceitos e Métodos. Oficina de Textos. https://repositorio.usp.br/directbitstream/b5f8d784-dfa9-40de-8857-add664ab3f88/Sanchez-2013-Avalia%C3%A7%C3%A3o_de_impacto_ambiental.pdf

[69] Ambrizzi, T., Rocha, R.P. da, Marengo, J.A., Pisnitchenco, I., Nunes, L.A. and Fernandez, J.P.R. (2007) Cenários regionalizados de clima no Brasil e América do Sul para o Século XXI: Projeções de clima futuro usando três modelos regionais (Relatório 3). Ministério do Meio Ambiente—MMA. http://mudancasclimaticas.cptec.inpe.br/~rmclima/pdfs/prod_probio/Relatorio_3.pdf

[70] Pilotto, I.L. (2015) Representação dos Efeitos de Heterogeneidades da Superfície sobre o Clima Local em uma Região de Paisagem Fragmentada na Amazônia Utilizando o Modelo Eta/Noah-MP. INPE. http://mtc-m21b.sid.inpe.br/col/sid.inpe.br/mtc-m21b/2015/07.29.21.37/doc/publicacao.pdf

[71] Umair, M., Kim, D. and Choi, M. (2020) Impact of Climate, Rising Atmospheric Carbon Dioxide, and Other Environmental Factors on Water-Use Efficiency at Multiple Land Cover Types. *Scientific Reports*, **10**, Article No. 11644. https://doi.org/10.1038/s41598-020-68472-7

[72] Pitman, A.J. (2003) The Evolution of, and Revolution in, Land Surface Schemes Designed for Climate Models. *International Journal of Climatology*, **23**, 479-510. https://doi.org/10.1002/joc.893

[73] D'Almeida, C., Vörösmarty, C.J., Hurtt, G.C., Marengo, J.A., Dingman, S.L. and Keim, B.D. (2007) The Effects of Deforestation on the Hydrological Cycle in Amazonia: A Review on Scale and Resolution. *International Journal of Climatology*, **27**, 633-647. https://doi.org/10.1002/joc.1475

[74] Pielke, R.A. (2001) Influence of the Spatial Distribution of Vegetation and Soils on the Prediction of Cumulus Convective Rainfall. *Reviews of Geophysics*, **39**, 151-177. https://doi.org/10.1029/1999rg000072

[75] Mahmood, R., Pielke, R.A., Hubbard, K.G., Niyogi, D., Dirmeyer, P.A., McAlpine, C., *et al.* (2013) Land Cover Changes and Their Biogeophysical Effects on Climate. *International Journal of Climatology*, **34**, 929-953. https://doi.org/10.1002/joc.3736

[76] Parween, N., Anamika, K. and Kumar, D.S. (2024) The Impact of Deforestation on Local Climates and Weather Patterns. *International Journal of Research Publication and Reviews*, **5**, 12170-12175. https://doi.org/10.55248/gengpi.5.0524.1431

[77] Dekker, S.C., O'connor, J.C., Staal, A., Tuinenburg, O.A., Rebel, K.T. and Santos, M.J. (2022) How Forests Transpiration and Interception Evaporation Can Buffer Variations in Precipitation Downwind. *EGU General Assembly* 2022, Vienna, 23-27 May 2022, EGU22-2794. https://doi.org/10.5194/egusphere-egu22-2794

[78] Barbarón, H.Y.S., Ildefonso, D.E.T. and Jimenez, D.M.G. (2024) The Relationship between Forest Cover Loss and Annual Rainfall in the Departments of Peru, 2013-2022. *Decision Science Letters*, **13**, 881-886. https://doi.org/10.5267/j.dsl.2024.8.004

[79] Pilotto, I.L., Rodríguez, D.A., Chan Chou, S., Tomasella, J., Sampaio, G. and Gomes, J.L. (2017) Effects of the Surface Heterogeneities on the Local Climate of a Fragmented Landscape in Amazonia Using a Tile Approach in the Eta/Noah-MP Model. *Quarterly Journal of the Royal Meteorological Society*, **143**, 1565-1580.

https://doi.org/10.1002/qj.3026

[80] Vale, R.S., Santana, R.A.S., Silva, J.T., Miller, S.D., Souza, R.A.F., Picanço, G.A.S., Gomes, A.C.S., Tapajós, R.P. and Pedreiro, M.R. (2016) Medições por covariância de vórtices turbulentos dos fluxos de calor latente, sensível, momentum e CO_2 sobre o reservatório da Usina Hidrelétrica de Curuá-Una—PA. Ciência e Natura v.38 Ed. *Especial-IX Workshop Brasileiro de Micrometeorologia*, Vo. 1, 15-20.

[81] Giambelluca, T.W., Ziegler, A.D., Nullet, M.A., Truong, D.M. and Tran, L.T. (2003) Transpiration in a Small Tropical Forest Patch. *Agricultural and Forest Meteorology*, **117**, 1-22. https://doi.org/10.1016/s0168-1923(03)00041-8

[82] Khanna, J., Medvigy, D., Fueglistaler, S. and Walko, R. (2017) Regional Dry-Season Climate Changes Due to Three Decades of Amazonian Deforestation. *Nature Climate Change*, **7**, 200-204. https://doi.org/10.1038/nclimate3226

[83] Sterling, S.M., Ducharne, A. and Polcher, J. (2012) The Impact of Global Land-Cover Change on the Terrestrial Water Cycle. *Nature Climate Change*, **3**, 385-390. https://doi.org/10.1038/nclimate1690

[84] Duarte, L.G., Romera, K., Sabino, M., Curado, L.F.A., Palácios, R.S. and Nogueira, J.S. (2018) Dinâmica dos fluxos de calor latente, calor sensível e fluxo de calor no solo no Pantanal Mato-Grossense. Anais 7º Simpósio de Geotecnologias no Pantanal, Jardim, MS, 20 a 24 de outubro 2018. Embrapa Informática Agropecuária/INPE, 431-440.
https://www.researchgate.net/publication/330637926_Dinamica_dos_fluxos_de_calor_latente_calor_sensivel_e_fluxo_de_calor_no_solo_no_Pantanal_Mato-Grossense

Appendix A

A.1. Eta Regional Model

The Eta regional model was adapted to perform long-term integrations (Pesquero *et al.*, 2010; Chou *et al.*, 2014a, b). Due to the higher resolution of the Eta regional model, it is possible to simulate mesoscale phenomena in greater detail, such as frontal systems, orography, sea breeze, severe storms, squall lines, and organized mesoscale systems (Chou, 1996). The dynamics of the regional model are developed using a vertical coordinate (η) in the form of discrete steps (Mesinger, 1984).

$$\eta = \left(\frac{P - P_t}{P_{sfc} - P_t} \right) * \eta_{sfc} \tag{1}$$

where:

$$\eta_{sfc} = \frac{P_{ref}\left(Z_{ref}\right) - P_t}{P_{ref}\left(0\right) - P_t} \tag{2}$$

where, η_{sfc} is the conversion from the sigma vertical coordinate (which follows the terrain) to the Eta coordinate (in the form of discrete steps); P_t is the pressure at the top of the domain; P_{sfc} and Z_{sef} are the pressure and elevation at the lower boundary of the model, respectively. The reference pressure (P_{ref}) is a function of the height above mean sea level.

The physical parameterizations included in the model are:

1) Turbulent processes in the atmosphere, represented by the Mellor-Yamada (1974) scheme, updated with the parameters of Nakanishi & Niino (2009), which calculates turbulent kinetic energy and vertical fluxes;

2) Turbulent energy diffusion in the surface planetary boundary layer (PBL), determined using the Mellor-Yamada 2.0 scheme (Mellor & Yamada, 1974);

3) The shortwave radiation scheme is based on the model by Lacis & Hansen (1974);

4) The longwave radiation scheme follows the model of Fels & Schwarzkopf (1975);

5) Precipitation in the model is produced by cumulus parameterization schemes proposed by Betts-Miller-Janjic (Janjic, 1994);

6) Cloud microphysics follows the approach described by Zhao *et al.* (1997);

7) The surface layer over land is resolved using the Monin-Obukhov scheme with stability functions from Paulson (1970), while the surface layer over the ocean uses the Charnock (1955) scheme;

8) Biosphere-atmosphere interaction processes are represented by the NOAH land surface scheme (Ek *et al.*, 2003), which distinguishes 16 vegetation types, 15 soil classes, and eight soil layers with roots extending to a depth of up to 12 meters (Pilotto *et al.*, 2023).

Table A1. Parameterizations included in the Eta-CPTEC regional model.

Parameter	Reference
Turbulent diffusion in the PBL	Mellor & Yamada (1974)
Shortwave radiation	Lacis & Hansen (1974)
Longwave radiation	Fels & Schwarzkopf (1975)
Cumulus parameterization	Betts-Miller-Janjic (Janjic, 1994)
Cloud microphysics	Zhao *et al.* (1997)
Surface layer (over land)	Monin-Obukhov-Paulson (Paulson, 1970)
Surface layer (over ocean)	Charnock (1955)
NOAH land surface scheme	Ek *et al.* (2003)

The land use and land cover map is derived from the ESA-CCI-LC (European Space Agency - Climate Change Initiative Land Cover) for the year 2000. The soil map is from STATSGO/FAO (State Soil Geographic/Food and Agriculture Organization) (Miller & White, 1998), with a spatial resolution of 1 km.

The model will be configured with 38 vertical levels, with the model top defined at 25 hPa. Time integration uses the split-explicit technique. The terms adjusted by inertial gravity waves are integrated separately from the advective terms. A forward-backward scheme handles the terms responsible for this adjustment (Janjic, 1979), while a modified Euler-backward scheme is applied to the horizontal and vertical advection terms (Janjic, 1984). The prognostic variables are: air temperature, specific humidity, horizontal wind, surface pressure, turbulent kinetic energy, and cloud hydrometeors. These variables are distributed on an Arakawa E-grid (Arakawa & Lamb, 1977), in which the distance between adjacent mass or wind points is used to define the model's horizontal resolution.

Appendix B

B.1. Bias

Bias indicates the systematic tendency of the simulations. In other words, if the bias is greater than zero, the forecasts are, on average, overestimated; whereas if it is less than zero, the forecasts are underestimated.

$$b = \frac{1}{N}\sum_{i=1}^{N}\left|\varphi_i - \psi_i\right|$$

B.2. Root Mean Square Error (RMSE)

The root mean square error (RMSE) method will also be used to assess the accuracy of the simulations, where high RMSE values indicate high levels of discrepancy between the simulations (ϕ) and the observed and reanalysis data (ψ). The RMSE formula is given by:

$$\mathrm{RMSE} = \left[\frac{1}{N}\sum_{i=1}^{N}\left|\varphi_i - \psi_i\right|^2\right]^{1/2}$$

Table A2. Monthly average values observed and simulated by the Eta model for Temperature (SAMeT) and Precipitation (CHIRPS) for the year 2021, and monthly observed averages for the period 2012 to 2021.

	Temperature (˚C)			Precipitation (mm·dia^{-1})		
	SAMeT 2012-2021	SAMeT 2021	Model 2021	CHIRPS 2012-2021	CHIRPS 2021	Model 2021
JAN.	26.11	25.68	25.74	9.75	12.50	5.89
FEB.	26.08	25.82	26.02	10.17	12.88	6.67
MAR.	26.23	25.51	26.02	10.89	12.47	6.70
APR.	26.23	26.14	25.91	10.06	11.52	6.12
MAY	26.3	26.25	25.84	7.28	6.12	5.09
JUN.	26.18	25.77	25.89	3.56	5.05	3.18
JUL.	26.2	26.14	25.96	2.68	2.67	2.51
AUG.	27.04	27.35	26.56	2.67	2.74	2.71
SEP.	27.26	27.01	26.65	4.24	5.18	3.50
OCT.	27.01	27.23	26.58	5.32	5.95	4.37
NOV.	26.79	26.39	26.29	8.06	8.52	4.85
DEC.	26.28	26.23	25.98	9.29	12.53	5.67

Table A3. Values found for bias and root mean square error for average temperature (˚C) at 2 m above ground level (SAMeT) and precipitation (mm·day^{-1}) (CHIRPS) in the simulation of the Eta regional model for the area influenced by highway BR-319.

	DJF	JJA	ANUAL 2021	ANUAL 2012-2021
BIAS - SAMeT	0.003	−0.287	−0.173	−0.356
RMSE - SAMeT	0.189	0.379	0.351	0.144
BIAS - CHIRPS	−3.267	−0.171	−3.405	−2.225
RMSE - CHIRPS	0.150	0.171	3.561	1.596

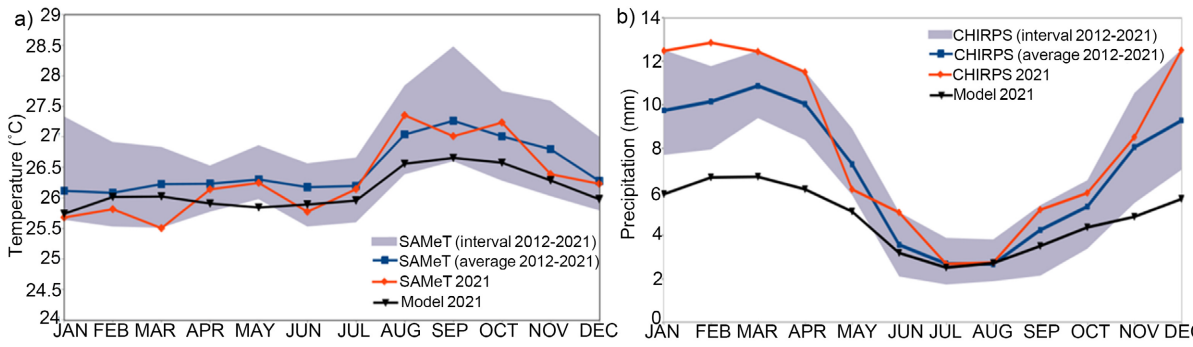

Figure A1. Seasonal cycle of (a) air temperature (˚C) at 2 m above ground level and (b) precipitation (mm·day^{-1}). The black lines correspond to the Eta model simulation (Model 2021); the lilac shaded area represents the standard deviation (2012-2021 observed climate range); the blue line is the mean (2012-2021 observed climate average); and the red line is the monthly observed mean for the year 2021.